UNIVERSIDAD DE SONORA

DIVISIÓN DE INGENIERÍA

DEPARTAMENTO DE INVESTIGACIÓN EN POLÍMEROS Y MATERIALES

SYNTHESIS OF Pd-Au BIMETALLIC NANOPARTICLES FOR APPLICATION IN CATALYSIS

T H E S I S

To obtain the academic degree of:

MAESTRO EN CIENCIA DE MATERIALES

Presents:

JAVIER ELISEO GALVEZ RAMIREZ

Hermosillo, Sonora, Mexico **February 2016**

This thesis has been performed in the Chemical Laboratories of Departamento de Investigación en Polímeros y Materiales de la Universidad de Sonora, under the direction of PhD. Judith Celina Tánori Córdova.

APPROVAL FORM

The members of the jury to review the Professional Thesis of JAVIER ELISEO GÁLVEZ RAMÍREZ, have found it satisfactory and recommend to be accepted as a partial requisite to obtain the Degree of Maestro en Ciencia de Materiales.

_____

PhD. Judith Celina Tánori Córdova
Departamento de Investigación en Polímeros y Materiales, Universidad de Sonora
Presidente

_____

PhD. Amir Darío Maldonado Arce
Departamento de Física, Universidad de Sonora
Secretario

_____

PhD. José Ronaldo Herrera Urbina
Departamento de Ingeniería Química, Universidad de Sonora
Sinodal

_____

PhD. María Elisa Martínez Barbosa
Departamento de Investigación en Polímeros y Materiales, Universidad de Sonora
Sinodal suplente

_____

PhD. Arturo García Bórquez
Escuela Superior de Física y Matemáticas, Instituto Politécnico Nacional
Sinodal externo

Acknowledgements

My deepest special thanks to **ANGEL**, who is the motor that runs my vehicle called life. To my **MOM**, who is always there supporting me in every step I take. To My **GRANDMA**, for showing me that to become the best means to be brave, symphatetic and enthusiastic in any situation. To my aunt and friend **ANA MARÍA**, for her powerful lessons in my life, for everything.

Thank you so much also to my supervisor, PhD **JUDITH**, for her support not only as my academic director but also as a person; for her understanding, teaching, training and sharing of life and proffesional experiences.

Thank you to **CONACYT** for supporting me financially and for allowing me to experience a summer scientific program abroad. Thank you also to CONACYT for funding this study through grant 242943.

Special thanks to the Transmission Electron Microscopy Laboratory at Centro de Nanociencias y Micro Nanotecnologias (CNMN) at Instituto Politecnico Nacional (IPN) and to the Transmission Electron Microscopy Laboratory at Universidad de Sonora, for provided services and micrograph published in the present work.

Thank you **GOD** for being always there showing me the path and how to make it good at any time.

God's timing is perfect

LIST OF ABBREVIATIONS

AOT	Bis(2- ethylhexyl)sulfosuccinate
Pd-Au	Palladium-Gold
CTAB	Cetyltrimethylammonium bromide
EDX	Energy-dispersive X-Ray spectroscopy
HAADF	High Angle Annular Dark-Field Z-Contrast Microscopy
HRTEM	High Resolution Transmission Electron Microscopy
NP	Nanoparticles
SDBS	Sodium dodecyl benzene sulfonate
SDS	Lauryl sodium sulfate
SEM	Scanning Electron Microscopy
SPRB	Surface Plasmon Resonance Band
STEM	Scanning Transmission Electron Microscopy
TEM	Transmission Electron Microscopy

CONTENTS

LIST OF FIGURES

LIST OF TABLES

ABSTRACT

The synthesis of Pd-Au bimetallic nanoparticles by sequential and simultaneous reduction of H_2PdCl_4 and $HAuCl_4$ with hydrazine in the reverse micelles of water/AOT/isooctane at 25 °C was investigated.

TEM photographs showed that the Pd-Au NP obtained at a feeding compositions of $[HAuCl_4]/ [H_2PdCl_4]$ = 2/1 by sequential reduction of Pd and Au, essentially had uniform sizes and mean diameters of about 5.7 nm. In case of simultaneous reduction of Pd and Au at a feeding compositions of $[HAuCl_4]/ [H_2PdCl_4]$ = 1/1, the NP had uniform sizes and smaller mean diameters of about 3.57 nm.

The UV-Vis absorption spectra for NP of palladium suggest that these NP reached their final sizes in less than 24 hours and the formation of Pd-Au bimetallic NPs in less than an hour because the palladium acts as a catalyst of gold during the reaction. The UV-Vis absorption spectra and X-ray diffraction patterns for the bimetallic systems of individual Pd NP suggest the formation of alloyed bimetallic NP, by both sequential and simultaneous reduction synthesis methods.

HRTEM photographs suggest the formation of alloyed bimetallic Pd-Au NP by both methods of synthesis.

EDX elemental analysis performed to Pd-Au NPs prepared by sequential reduction and the result showed a nanoparticle composition of 76.37 % of Au and 7.77 % of Pd.

STEM-HAADF and EDX analysis of Pd-Au Nps prepared by the simultaneous reduction method suggest the formation of Pd-Au alloyed bimetallic NP, where gold and palladium are well dispersed in the NP and sometimes more gold or palladium can be found in the core of the NP.

Chapter 1. Introduction

Bimetallic NP, such as nanoalloys or nanocomposites, are a class of important materials receiving considerable attention because of their unique properties. In many cases, the specific properties of bimetallic NP are enhanced because of the synergistic effects of two distinct metals. Nanoalloys are metallic clusters composed of two or more metal elements, and their physical and chemical properties are defined not only by their size and stoichiometry (atomic arrangement) but also by their challenging composition, (Kharisov et al., 2012). Nanocomposites are materials that incorporate nanosized particles into a matrix of standard material, encompass a large variety of systems such as one-dimensional, two-dimensional, three-dimensional and amorphous materials, made of distinctly dissimilar components and mixed at the nanometer scale, (AZoNano, 2005). Moreover, the diversity in structures, compositions, and properties of bimetallic NP enable their widespread applications in various fields, such as catalysis, electrochemistry, magnetism, optics and biomedicine. These applications often highly depend on the NP structure (e.g.,shape, size, composition and surface chemistry), (Liu et al., 2014).

A wide range of techniques have been developed for the preparation of NP and nanomaterials. These techniques include physical methods such as mechanical milling (Arbain et al., 2011) and inert gas condensation (Pérez-Tijerina et al., 2008), along with chemical methods such as chemical reduction (Song et al., 2009), photochemical reduction (Ghosh et al., 2002), electrodeposition (Mohanty, 2011), hydrothermal (Hayashi & Hakuta, 2010), and sol-gel synthesis (Sonawane & Dongare, 2006). Among all chemical methods the microemulsion has been demonstrated as a very versatile and reproducible method that allows to control over the nanoparticle size and yields NP with a narrow size distribution (LopezQuintela, 2003).

Au-Pd bimetallic NP have proved to be excellent catalysts for a variety of reactions with superior activity and durability to their monometallic counterparts (Zhan et al., 2011). Au-Pd catalysts have been of particular interest not only because of the wide range of reactions in which they can be used but also because of their relative simplicity. Au and Pd are soluble at

all compositions, so that the effects of different phases need not be considered. In many reactions, Au is catalytically inert, so any catalytic activity has be ascribed to Pd, (Wilson et al., 2013).

Supported Au and Pd nanoparticle catalysts have been investigated intensively since the first succesful CO oxidation over Au and the application of Pd in catalyzing aerobic oxidation of alcohol. Bimetallic NP are of greater interest than monometallic ones for improving catalytic properties due to synergetic effects between two elements. Recently, several research groups have examined supported Au-Pd bimetallic catalysts, which have remarkably enhanced catalytic activity and product selectivity in various alcohol oxidation reactions. The advantage of bimetallic catalysts is attributed not only to electronic interaction between the two metals but also to the complex structure of bimetallic NP (Chen et al., 2012).

The aim to this thesis has been to improve the synthesis route for a bimetallic Pd-Au nanoparticle in water-in-oil- microemulsions and its characterization.

Here, it is studied the preparation of Pd-Au NP in water-in-oil microemulsions. The microemulsions are created in the ternary system water/aerosol OT/isooctane. The NP are prepared by the sequential and simultaneous reduction of the tetrachloropalladate (II) and tetrachloroaurate (III) ions with hydrazine. The experimental method has been based in the synthesis of core-shell (Pd-Au) bimetallic NP in microemulsions by Larios et al., 2012.

The characterization of the NP has been carried out with UV-Vis spectroscopy, Transmission Electron Microscopy, High Resolution Transmission Electron Microscopy, Energy-dispersive X-Ray spectroscopy and High Angle Annular Dark-Field Z-Contrast Microscopy.

This thesis consists of 7 chapters: 1. Introduction, 2. Background, 3. Objectives of the thesis, 4. Materials and methods, 5. Results and discussion, 6. Conclusions and 7. Recommendations and further research.

Chapter 2. Background

2.1 Nanoparticles

A nanoparticle is defined as a particle in the nanoscale size range 1-100 nm (1nm=1x10^{-9} m). In the case of transition metal NP, the decreasing in size to the nanometre length scale increases the surface-to-volume ratio. This, together with the ability to prepare them in different sizes and shapes, makes them potentially useful in the field of catalysis (Cookson, 2010). NPs have shown to possess structural, electronic, dielectric, magnetic, optical and chemical properties that are different from the corresponding bulk materials (Jellinek, 2008). The systematic adjustment of the reaction parameters such as reaction time, temperature, concentration and the selection of reagents and surfactants can be used to control the size and shape of NP. (Burda et al., 2005).

2.2 Microemulsions

Microemulsions are homogeneous in macroscale and microheterogeneous in nanoscale dispersion of two immiscible liquids consisting of nanosized domains of one or both liquids in the other, stabilized by an interfacial film of surface active molecules. Microemulsions are macroscopically homogeneous mixtures of oil, water, and surfactant, which on the microscopic level consist of individual domains of oil and water separated by a monolayer of amphiphile (Kronberg et al., 2014). Microemulsions are thermodynamically stable, single optically isotropic and usually form spontaneously, (Zielińska-Jurek et al., 2012).

Microemulsions have ultralow interfacial tension, large interfacial area and capacity to solubilize both aqueous and oil-soluble compounds. Depending on the proportion of various components and hydrophilic–lypophilic balance value of the used surfactant microemulsions can be classified as water-in-oil, oil-in-water and intermediate bicontinuous structural types that can turn reversibly from one type to the other. The dispersed phase consists of monodispersed droplets in the size range of 5 – 100 nm. The nanodroplet size can be modified by varying concerned parameters, e.g. the type of stabilizer, continuous phase, the precursor content dissolved within the nanodroplets, and the water content, referred to as molar ratio of water to surfactant (W). In addition the stability of the microemulsion can be

influenced by addition of salt, concentration of reagents, temperature or pressure, (Zielińska-Jurek et al., 2012).

2.2.1 Preparation of nanoparticles in microemulsion system

The preparation procedure of metallic NP in W/O microemulsion commonly consists of mixing of two microemulsions containing metal salt and a reducing agent, respectively as shown in Figure 1A.

After mixing two microemulsions, the exchange of reactants between micelles takes place during the collisions of water droplets result of Brownian motion, the attractive van der Waals forces and repulsive osmotic and elastic forces between reverse micelles. Successful collisions lead to coalescence, fusion, and efficient mixing of the reactants. The reaction between solubilizates results in the formation of metal nuclei. Bönnemann et al. reported that at the initial stage of the nucleation, metal salt is reduced to give zerovalent metal atoms, which can collide with further metal ions, metal atoms, or clusters to form an irreversible seed of stable metal nuclei (Bönnemann & Richards, 2001). Growth then occurs around this nucleation point where successful collision occurs between a reverse micelle carrying a nucleus and another one carrying the product monomers with the arrival of more reactants due to intermicellar exchange. The nucleation reaction and particle growth take place within the micelles and the size and morphology of as-prepared NP depend on the size and shape of the nanodroplets and the type of the surfactant, whose molecules are attached on the surface of the particles to stabilize and protect them against further growth, (De Windt et al., 2005).

Another method to prepare NP is from a single microemulsion as shown in Figure 1B and 1C. One of the reactants usually a precursor of metal NP is solubilised inside reverse micelles and the second reactant (often a reducing agent) added directly to the microemulsion system. For the NP formed in single microemulsions the mechanism is based on intramicellar nucleation and growth and particle aggregation. This method was applied for the first time by Boutonnet et al. in 1982 for preparation of Pt, Rh, Pd and Ir NP in W/O microemulsion. Metallic NP were formed in single microemulsions using CTAB or Poly(ethylene glycol) diglycidyl ether (PEGDE) as a stabilizer. The precursors composed of water-soluble metal

salts and hydrogen gas, bubbled through the microemulsion, or hydrazine, were added directly to the microemulsion, as the reducing agent (Boutonnet et al., 1982).

Husein et al. described that intramicellar nucleation and growth dominate when high reactant occupancy numbers are coupled with rigid surfactant layer, while intermicellar nucleation and growth dominate at low occupancy numbers and less rigid surfactant layers. At intermediate values of occupancy the number and surfactant layer rigidity, both intramicellar and intermicellar nucleation and growth contribute to the final particle size and polydispersity (Husein & Nassar, 2008).

Sanchez-Dominguez et al. prepared Pt, Pd and Rh NP by an oil-in-water microemulsion reaction method. The microemulsion containing metal precursor (Pt-COD, Pd-AAc, Rh-COCl) was prepared by mixing appropriate amounts of surfactant, cosurfactant(s), oil phase and deionized water. The used systems: water/ Tween 80/Span 20/1,2-hexanodiol/ethyl oleate (System A); water/Brij 96V/butyl-S-lactate (System B) and water/Synperonic 10/5/isooctane (System C). Then to the solutions, under vigorous stirring at 25°C, a small amount of an aqueous solution of sodium borohydride was added (Sanchez-Dominguez et al., 2009).

2.2.2 Effects of the parameters on the formation of nanoparticles in microemulsion

The formation of NP in the microemulsion system is a strong function of the intermicellar exchange, which is denoted by the intermicellar exchange rate coefficient (kex) and affected by many factors such as: the type of continuous phase, the precursor content dissolved within the nanodroplets, and the water content, referred to as molar ratio of water to surfactant (W). The high exchange rate between the micelles yields large numbers of NP with a relatively small diameter. On the contrary, slow exchange of materials between the micelles leads to formation of a few numbers of nuclei and results in larger final particle size.

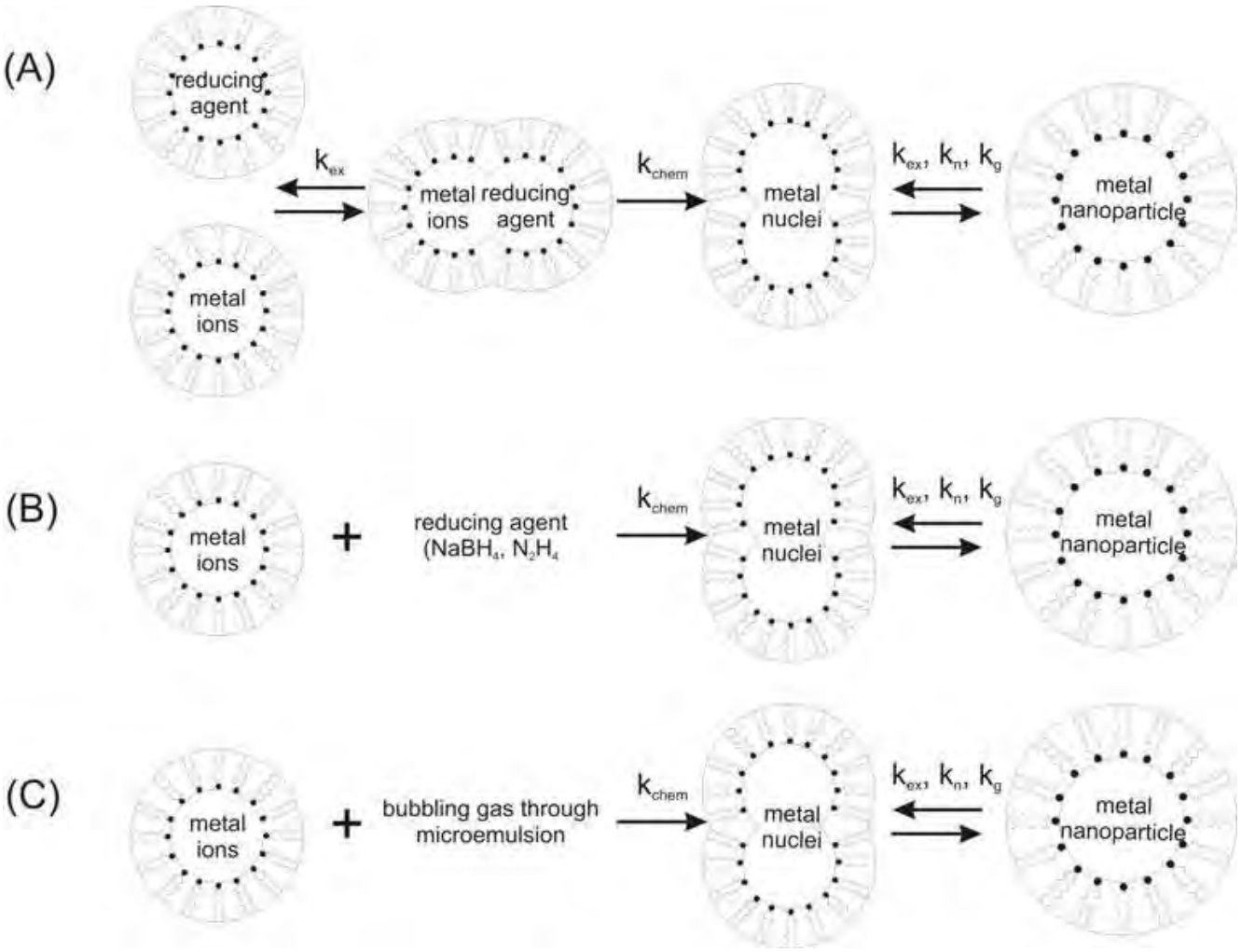

Figure 1. Schematic illustration of NP preparation using microemulsion techniques: Particle formation steps. k_{chem} is the rate constant for chemical reaction, k_{ex} is the rate constant for intermicellar exchange dynamics, k_n is the rate constant for nucleation, and k_g is the rate constant for particle growth (Zielińska-Jurek et al., 2012).

The second studied parameter which can influence the nanoparticle size and shape is the type of the surfactants and the addition of the co-surfactants. The surfactants consist of two main entities, a hydrophilic head group and a hydrophobic (or lypophilic) tail group, which form soft aggregates in solvents and are held together by van der Waals and ionic forces.

The surfactant acts as a stabilizing agent, effectively dispersing the obtained NP in the solution, providing sites for the particle nucleation and preventing aggregation of the NP. In W/O microemulsions surfactants form reverse micelles, nano-sized water pools dispersed within the bulk organic solvent which act as nanoreactors for the chemical reduction of the metallic precursors and metallic nanoparticle preparation.

For the most surfactant-mediated synthesis, the connection between morphology of the surfactant aggregates and the resulting particle structure is more complex (than simply relating the average size and shape of the micelles to the size and shape of the precipitated particles).

Usually, many surfactants can be used to form microemulsion, including cationic surfactants such as CTAB, anionic surfactants such as AOT, SDBS and SDS, and nonionic surfactants such as Triton X-100 and sorbitan monooleate Span 80, nonylphenyl ether (NP-5) or polyoxyethylene (9) nonylphenyl ether (NP-9).

The most commonly used surfactant for the formation of reverse micelles is the sodium bis(2-ethylhexyl) sulfosuccinate, also known as Aerosol-OT or AOT, seen in Figure 2. AOT is a twin tailed, anionic surfactant with a sulfosuccinate head group stabilized as a salt by a sodium cation. The AOT molecule has an inverted conical shaped structure and has proven to be an effective emulsifier, thus finding a wide range of applications as well as numerous intensive studies. The surfactant layer acts as steric stabilizer to inhibit the aggregation of NP formed. The microemulsion formed by AOT is made up of three kinds of components AOT, water, alkane (without addition of co-surfactants). In this system, micelles consist of a hydrophilic core compartmentalised by the hydrophilic head group of the AOT, forming a “water-pool” characterized by the molar ratio of water to surfactant (W= $[H_2O]/[AOT]$) and with the hydrophobic alkyl tails extending into the nonpolar continuous phase solvent.

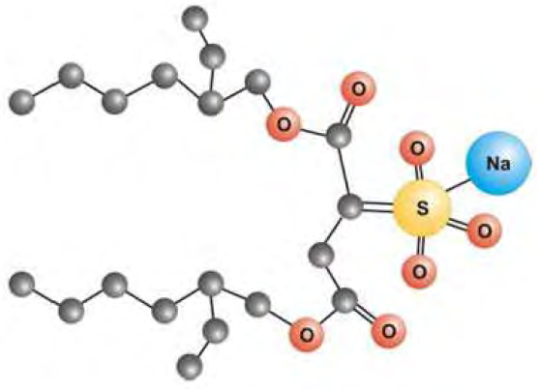

Figure 2. Model of surfactant AOT molecule (Zielińska-Jurek et al., 2012)

AOT microemulsion has extensively been applied for preparation of metallic NP (Pt, Pd, Cu, Ag, Au, Ni, Zn), metal sulfides (CdS, ZnS) and metal oxides (TiO_2, SiO_2). The resultant particles have high stability, small particle size, and good monodispersity. Due to its higher solubility in organic phase AOT helps to extract metal cations from the aqueous to reverse micellar phase. In addition the particles formed in AOT microemulsion have relatively strong electrostatic interactions with the negatively charged head polar group of AOT molecules, which comes into being a protective effect against aggregation (Zhang et al., 2007).

Zhang et al. (Zhang et al., 2007; Zhang et al., 2006) reported that silver NP prepared in AOT microemulsion have a smaller average size and narrower size distribution compared to the particles prepared using cationic or nonionic surfactant in the microemulsion system (Zhang et al., 2007). In addition, due to the adsorption of AOT molecules onto the particles, the resultant sol can be preserved for a long time without precipitation and it easily transfers the obtained NP into nonpolar solvents (Zhang et al., 2006).

Solanki et al. studied the effects of reaction parameters, including water-to-surfactant ratio (W), type of continuous oil phase in water/AOT/cyclohexane microemulsion system. They found that silver NP were smaller and narrower in the size distribution at lower water content than that obtained at higher W value. When W values increased from 5 to 8 the particle size increased from 4–9 nm to 50–58 nm (Solanki et al., 2010).

Chen et al. prepared platinum ultrafine particles by the reduction of H_2PtCl_6 with hydrazine in AOT/isooctane microemulsion system. They have found that the hydrodynamic diameters of reverse micelles measured by DLS increased with the increase of W values. When the aqueous phase was the solution of 0.1 M H_2PtCl_6 or 1.0 M hydrazine, it was observed that the reverse micellar sizes were smaller than those obtained using water as the aqueous. It could be attributed to the fact that the dissociation of H_2PtCl_6 or hydrazine in solution caused the increase of ionic strength, which reduced the repulsion between the head groups of ionic surfactant and led to the formation of smaller reverse micelles. The formation rate was faster at larger W values. This could be attributed to the fact that the number of nuclei formed in aqueous phase increased as the W value increased at constant AOT and H_2PtCl_6 concentrations, leading to the increase in the formation rate (Chen et al., 1999).

Wu et al., investigated the synthesis of Au/Pd bimetallic NP at various molar ratios by the coreduction of $HAuCl_4$ and H_2PdCl_4 with hydrazine in the reverse micelles of water/AOT/ isooctane at 25 °C. The characterization and formation kinetics of particles suggested that (1) most of $AuCl_4^-$ and $PdCl_4^{2-}$ ions were reduced before the formation of nuclei, (2) the nucleation rate of Au was much faster than that of Pd, (3) the size of bimetallic NP was determined by the number of the nuclei formed at the very beginning of reaction, and (4) the nuclei for the bimetallic system might be composed of Au and Pd. According to these suggestions, a formation process of Au/Pd bimetallic NP was proposed (Wu et al., 2001).

2.3 Palladium nanoparticles and catalysts

It has been shown that Pd NP can be produced by the metal respiring bacterium *Shewanella oneidensis* in presence of a hydrogen donor. In this context, NP of Pd supported on the cell wall and periplasmatic structures of the bacteria are referred to as bio-Pd (De Windt et al., 2005). Since the bacteria mediate the reduction process and as a support for the resulting NP, fewer chemicals are involved in the production process, which makes the process safer and less expensive. Therefore, these biological synthesis methods can be a valuable alternative for chemical methods. Biosupported Pd NP have been shown to catalyze the dehalogenation of a number of important environmental contaminants, while the degradation of other chlorinated compounds such as 1,2-dichloroethane are not catalyzed by current formulations of Pd catalysts (McNab et al., 2000).

Combining biosupported Pd NP with other elements to multimetallic structures could be an option to improve the catalytic activity. Recently the synthesis of a Pd-on-biomagnetite catalyst was reported (Coker et al., 2010). More specifically, magnetite crystals were produced extracelullarly by *Geobacter sulfurreducens* by reduction of Fe(III)-oxyhydroxide. After synthesis of the biomagnetite, Pd(II) was added and reduced chemically on the surface of the biomagnetite crystals.

Pd catalysts have been studied extensively for their potential use as catalysts for the hydrodehalogenation in organic synthesis and pollutant degradation (Aarts et al., 1989) Pd catalysts doped with other metals for the creation of bimetallic nanoparticle catalysts have shown enhanced activity, which has been attributed to changes in geometric and electronic

properties (Coq, 2001). For example, an alloyed Pd/Au catalysts produced by coprecipitation was shown to promote the oxidation of CO (Venezia et al., 2003). A Pd/Au on carbon catalyst, which was produced by reducing Pd and Au sequentially, was able to catalyze the dechlorination of CCl_2F_2, which enhanced selectivity for CH_2F_2 (Bonarowska et al., 2001). A bimetallic core-shell structure, consisting of Au-core with a Pd-shell was shown to increase the activity of Pd NP for the hydrodechlorination of trichloroethylene by a factor 15 (Nutt et al., 2005). All of these catalysts were produced using chemical synthesis methods that require the use of expensive substances, such as stabilizers (e.g., polyvinylpyrrolidone) and carrier materials (e.g., Al_2O_3, activated carbon). Palladium NP can be produced using the following methods: solution thermolysis, sonochemical methods, electrochemical methods and radiolysis (Kim et al., 2006).

2.4 Gold nanoparticles

Gold NP are of interest as a potential core for bimetallic core-shell NP, as they are more economically viable than the metals that are generally used for catalysis. Gold particles are not difficult to synthesize. Zhao and Xu chose gold as a core for their Au-Pt core-shell NP because it is inert in acid electrolytes and its surface favours deposition of platinum (Zhao, 2006).

Brown et al. synthesized gold NP of mean diameter 2.6 to 100 nm, using a seeding technique. They compared the use of citrate and hydroxylamine as reductants. The citrate seeded particles were highly uniform in size; however, the hydroxylamine seeded gold colloids produced two distinct populations of large spheres and small rods (Brown et al., 2000). They found that the 2.6 nm diameter seeds had a standard deviation of ~1 nm. The citrate method of developing gold NP was first developed by Turkevich et al. This is one of the best-known methods for producing gold NP and involves reducing $HAuCl_4$ with sodium citrate. The citrate acts as the reductant and as the stabiliser (Turkevich et al., 1951).

2.5 Bimetallic nanoparticles

Bimetallic NP are the combination of two metals of the nanoscale size range. This area of nanoscience is of interest in the field of catalysis as bimetallic NP can exhibit synergistic effects.

Bimetallic NP can be classified into four types of mixing patterns: core-shell, sub-cluster, mixed and multishell NP. Core-shell NP consist of a shell of one type of atom surrounding a core of another type of atom (Ferrando et al., 2008).

2.6 Au-Pd bimetallic nanoparticles

Among the bimetallic NP, gold-palladium (Au-Pd) is one of the most attractive systems because of its promising use as a catalyst in CO oxidation, vinyl acetate monomer synthesis, hydrodechlorination of $CClF_2$, hydrogenation of hydrocarbon, cyclotrimerization of acetylene and so forth (Chen et al., 2005).

There are normally two approaches to synthesize Pd-Au bimetallic NP: sequential and simultaneous reduction of the metallic precursors (Fan et al., 2008). The sequential reduction approach normally gives better control of the shape and atomic ratio as compared to the simultaneous approach, and the synthesized Pd-Au bimetallic NP show core-shell structure. The chemical activity of these NP is strongly determined not only by the particle size but also by the Au/Pd ratio at the surface (Liu et al., 2005). Therefore, it is needed to characterize whether the Au and Pd components are chemically segregated or intimately alloyed in the synthesized NP. According to the phase diagram, Au-Pd is likely to form solid solutions of arbitrary composition (Okamoto et al., 1985). Further, the catalysts are normally used at high temperatures; thus, the structure ability and the species diffusion configuration are also important issues that need to be clarified (Chen et al., 2005).

A number of methods have been developed for synthesizing Au(core)-Pd(shell) bimetallic NP. Knecht et al. have discussed different ways of forming Au-Pd bimetallic NP. The reduction of metallic precursors can either by initiated by the polyol method or by addition of borohydride. The polyol reduction often results in the formation of Au(core)-Pd(shell) NP, because of the difference in the reduction potentials of gold and palladium. The gold is easier to reduce and provides a seed for the palladium to be reduced on. The sizes of the core and shell can be controlled by the ratio of gold:palladium used during synthesis (Knetch et al., 2008).

Kim et al. synthesized Au(core)-Pd(shell) by first producing monodispersed goldcore particles having approximately 75 nm diameters, by conventional citrate reduction. These cores were coated with Pd to give core-shell particles with diameters in the range of 100 to 600 nm, with controllable Pd shell thickness (Kim et al., 2006).

2.7 Characterization of bimetallic nanoparticles

The size, shape and morphology of NP play an important role on their chemical properties. Therefore, it is very important to have means of characterizing their physical properties.

2.7.1 UV-Vis spectroscopy in Au and Pd nanoparticle characterization

UV-Vis spectroscopy can be used to determine size and elemental information from coloidal sols of metallic nanoparticle system. The UV-Vis absorption spectra of a metal nanoparticle system is dependent of the size of the nanoparticle (Cookson, 2009).

When synthesizing NPs of metals which have visible plasmon bands it is useful to monitor the change in the UV-Vis spectra in order to determine that the metal has been successfully reduced. Although this is often accompanied by a visible colour change, the change in the UV-Vis spectrum will provide evidence that all of the metal precursor has been reduced, as well as provide some indication of the NP shape. If a NP is of zeroth dimension (i.e. spherical) it will only have one plasmon band. This is because all the directions in which the electrons can oscillate are equivalent. Two or three dimension particles such as rods or prisms produce UV-Vis spectra with two or three absorption peaks, respectively. The formation of multiple resonance bands is due to the propagation of electrons in multiple directions (Cao, 2004).

Turkevich et al. have demostrated that coloidal gold has an absorption maximum at 522 nm, which falls to half the value of the maximum at 470 nm and steadily rises into the ultraviolet to the limits of detection at 210 nm. It was also shown that as the size of the gold nanoparticle increased, the absorption maximum gradually shifts to the red (Turkevich, 1951). When Turkevich et al. examined gold NP with irregular shapes, the absorption band became flattened (Creighton et al., 1991).

Kim et al. recorded a λ_{max} at 230 nm for their palladium particles, which is characteristic for palladium NP less than 10 nm in size. They also recorded a plasmon absorption band at 560 nm for the citrate reduced gold NP around 75 nm in diameter. They found that the gold absorption band disappeared completely as the palladium shell formed (Kim et al., 2006).

Lopez-Sanchez et al. recorded UV-Vis spectra for Au and Pd sols in water. For the Au sols, they found a plasmon resonance band at 505 nm, characteristic of gold NP of a size below 10 nm. The Pd sols displayed no surface plasmon band (Lopez-Sanchez et al., 2008).

2.7.2 UV-Vis spectra in Au-Pd core-shell nanoparticle characterization

Ferrer et al. analyzed their Au(core)-Pd(shell) bimetallic NP with UV-Vis spectroscopy and they found a very pronounced absorption band at 550 nm, characteristic of Au, but by increasing the concentration of Pd, the intensity of the surface plasmon resonance band associated with Au (525 nm) faded away (Ferrer et al., 2007).

In the synthesis of bimetallic NPs with Au seeds, one can analyse the spectrum of the seed NP before the addition of the second metal. Once the second metal is reduced onto the seed particle, the UV-Vis spectra can then be collected and the difference between the two can be analyzed. In the case of Au-Pd NPs, the addition of Pd to the Au surface dampens the plasmon band produced by Au. This is because the plasmon band of NPs is surface dependant; therefore once the particle is covered by a Pd shell the plasmon band from Au is dampened. As Pd does not have a plasmon band in the visible region of the spectrum, the spectrum of the bimetallic NPs have no visible absorption band. If the characteristic plasmon band of Au still appears in the UV-Vis spectrum after the reduction of Pd, it may be indicative that there are monometallic Au NPs still present in the system. Therefore, the Pd would not have been successfully reduced onto the Au seeds. This method of analysis was performed by Scott et al. in the formation of Au-Pd bimetallic NPs (Scott et al., 2004).

Lopez-Sanchez et al. found that when they mixed the Au and Pd sols they had previously produced, the spectrum of a mixture of the two metals sols indicated the disappearance of the Au surface plasmon band. (This indicated that the Pd was dominating the optical properties of the mixture (Lopez-Sanchez et al., 2008).

2.7.3 Transmission Electron Microscopy

TEM is a common technique used to determine the size, geometry, and crystal shape of NP (Cao, 2004). In this form of microscopy, high energy electrons are directed at and passed through a very thin sample of material. The atoms within the material absorb or scatter the incoming electrons (Egerton, 2005). Common TEM imaging techniques include dark field and bright field imaging. The difference between these two techniques is determined by the source of electrons that are imaged. If the non-scattered/absorbed electrons are imaged, they will appear as a bright spot on the film. This essentially creates a shadow image of the material being analyzed. Therefore the background or "field" which consists of non-absorbed/scattered electrons will form a bright field image, leaving the image of the sample as a dark spot, much like a shadow. Imaging the electrons diffracted by the sample produces a dark-field image. The areas which diffract electrons will appear to be bright spots on the film, leaving areas which did not diffract electrons dark. Dark and light field images are essentially the same image with opposing contrasts (Yasar-Inceoglu et al., 2012).

Since NPs are composed of metals which are high in electron density, there is a high contrast between the metal NP and the carbon TEM grid over which it is placed. Therefore, the NPs are easily detected by TEM and the size and geometry of the particles can clearly be seen in the resulting image. NP sizes are measured from the image, often with the aid of imaging programs and particle size counting programs such as Image J (Schneider et al., 2012). If enough particles are analyzed, information about the average size and distribution of the particles can be calculated. This information is invaluable for NP analysis and characterization since properties such as catalytic ability and selectivity depend highly on their size and structure (Frenkel et al., 2001). Unfortunately, when a bimetallic NP is composed of two similar metals such as Au-Pd or Au-Pt, the electron densities are often too similar to detect any difference in contrast. Thus, only the size and shape of this type of NP can be detected (Shevchenko et al., 2008).

2.7.4 Energy-dispersive X-Ray spectroscopy

Backscattered electron images in the SEM display compositional contrast that results from different atomic number elements and their distribution. EDX allows us to identify what those particular elements are and their relative proportions (atomic %, for example).

Initial EDX analysis usually involves the generation of an X-ray spectrum from the entire scan área of the SEM. In a X-ray spectra generated from an entire scan area, the Y-axis shows the counts (numer of X-rays received and processed by the detector) and the X-axis shows the energy level of those counts (Hafner, 2016).

2.7.5 HAADF Microscopy

HAADF images are formed by collecting high-angle scattered electrons with an annular dark-field detector in dedicated STEM instruments. The contrast of HAADF images is (a) strongly dependenf on the average atomic number of scatterer encountered by the incident probe; (b) not strongly affected by dynamical diffraction effects; (c) not strongly affected by defocus; and (d) not strongly affected by sample thickness variations. Spatial resolution is limited by the size of the focussed incident probe (LE-CSSS, 2016).

Samples must be thin (<40 nm) for most high resolution imaging applications. The limitations of HAADF imaging is only quasi-spectroscopic. The image resolution is not as high as that of HRTEM images. Thick specimens beam broadening and degradation of the spatil resolution. HAADF images have a much poorer signal-to-noise compared to HRTEM images (LE-CSSS, 2016).

Chapter 3. Objectives of the thesis

3.1. Main objective

Improve the synthesis route of a bimetallic Pd-Au nanoparticle in water-in-oil- microemulsions by sequential and simultaneous reduction of Pd and Au ions, and characterize the obtained NP.

3.2. Specific objectives

- Synthesize and characterize monometallic Pd NP.
- Synthesize bimetallic Pd-Au NP in water-in-oil microemulsions by sequential reduction of Pd and Au.
- Synthesize bimetallic Pd-Au NP in water-in-oil microemulsions by simultaneous reduction of Pd and Au.
- Characterize the bimetallic Pd-Au NP synthesized, via UV-Vis Spectroscopy, TEM, HRTEM and EDS Spectroscopy, by sequential and simultaneous reduction of Pd and Au.
- Determine the type of nanoparticle obtained by sequential and simultaneous reduction of Pd and Au: core-shell or alloy
- Determine the average size and the particle size distribution of bimetallic Pd-Au NP synthesized by sequential reduction of Pd and Au.
- Determine the average size and the particle size distribution of bimetallic Pd-Au NP synthesized by simultaneous reduction of Pd and Au.

Chapter 4. Materials and Methods

This chapter details the experimental methods used in this thesis to produce and characterize bimetallic NP of less than 10 nm diameter in size.

4.1. Sequential reduction of Pd and Au for synthesis of Pd-Au nanoparticles.

4.1.1 Reagents.

- Hydrogen tetrachloroaurate (III) hydrate ($HAuCl_4$)
- Tetrachloropalladate acid (H_2PdCl_4), prepared with $PdCl_2$ and HCl
- Aerosol OT (AOT or sodium bis(2-ethylhexyl) sulfosuccinate
- Isooctane
- Hydrazine (N_2H_4)
- Dodecanethiol [$CH_3(CH_2)_{11}SH$]

4.1.2 Microemulsions

The bimetallic NP have been synthesized in the aqueous domains of microemulsions of the ternary system water-aerosol OT-isooctane. The phase diagram of the system can be found in the research of Tamamushi et al., 2009. The oil phase in the microemulsion is isooctane. In addition, ultrapure water from a Milli Q system was used. The NP were prepared in the reactor environment defined by the aqueous domains of reverse micelles following the method described by Larios et al., 2012. These micelles are water droplets suspended in isooctane, stabilized by an AOT monolayer. The synthesis was performed in micelles with a surfactant concentration of 0.1 M (in isooctane). Water was added to form the microemulsion, until a water-surfactant concentration ratio, $w = [H_2O] /[AOT] = 5$ was obtained.

4.1.3 Preparation of palladium seeds by the sequential method

The synthesis of Pd seeds was made following the method described by Larios et al., where metallic ions were introduced as an aqueous 0.2 M solution of H_2PdCl_4, prepared by dissolving $PdCl_2$ in a 0.2 N HCl solution. An amount of 1 µL of this solution was added per 1 mL of microemulsion. The reducing agent was hydrazine (1 µL per 3 mL of

microemulsion). The reaction proceeded in the water pool after hydrazyne addition. The metallic precursor was reduced to its zero-valence state, and then the Pd NPs formed by aggregation. These Pd particles have served as seeds.

4.1.4 Addition of gold

The obtained Pd NP from section 4.1.3 were used as preformed cores for the preparation of bimetallic Pd-Au NP. An aqueous 0.2M solution of $HAuCl_4$ (2 µL per 1 mL of microemulsion) was added into the reaction system containing the Pd seeds under stirring. Afterwards, hydrazine was added to the system under vigorous stirring as a reductant. The bimetallic NP were obtained as a purple-brown suspension. The Pd:Au molar ratio was 1:2.

4.1.5 Preparation of passivated bimetallic Pd-Au nanoparticles

The surface of the Pd-Au NP was passivated in order to stabilize them against coagulation and/or coalescence. For this, it was adsorbed the functional -SH thiol group of dodecanethiol onto the gold surface of the NP. When the Pd-Au NP were obtained, it was added to the solution 9 µL of dodecanethiol per mL of microemulsion.

4.2 Simultaneous reduction of Au and Pd for synthesis of Pd-Au nanoparticles

The NP have been synthesized in the aqueous domains of microemulsions of the ternary system water-aerosol OT-isooctane. The aqueous solutions of H_2PdCl_4 and $HAuCl_4$ were added simultaneously to the microemulsion. After mixing these solutions, hydrazine was added for the reduction of both Pd and Au, respectively. Some minutes after, thiol was added to passivate the NPs formed.

4.3 Characterization of Pd and Pd-Au nanoparticles

The NP were characterized in a JEOL JEM 2010 F transmission electron microscope. A drop of each sample was placed on a carbon film supported by a copper grid in order to obtain TEM micrographs. It has further analyzed the bimetallic structures by means of high resolution TEM images. The optical properties of the samples were investigated by UV-Vis spectroscopy. EDX was used to determine the elements forming the NP.

The UV-Vis spectra were obtained with the Agilent 8453 UV-Vis spectrophotometer (two-diode array, its radiation source is a combination of a deuterium-discharge lamp for the ultraviolet (UV) wavelength range and a tungsten lamp for the visible and short wave near-infrared (SWNIR wavelength range). The samples were placed in 1 x 1 x 3 cm rectangular quartz cells. Different samples were analyzed in the spectrophotometer:

Number	Reference	Sample
1	isooctane	AOT-isooctane
2	isooctane	AOT-isooctane-H_2O
3	AOT-isooctane	AOT-isooctane-H_2O-H_2PdCl_4-N_2H_4
4	AOT-isooctane-H_2O	AOT-isooctane-H_2O-H_2PdCl_4-N_2H_4-$HAuCl_4$
5	AOT-isooctane-H_2O	AOT-isooctane-H_2O-H_2PdCl_4-N_2H_4-$HAuCl_4$-thiol

Chapter 5. Results and discussion

5.1. Sequential reduction of Pd and Au for synthesis of Pd-Au NP

The results obtained of the more remarkable experiments are explained taking into consideration the different synthesis performed and their respective chemical and physical characterization: UV-Vis spectroscopy, TEM, HRTEM and EDX Spectroscopy.

There is a variation of colors depending on the synthesis step. The prepared H_2O-AOT-isooctane microemulsion is a colorless liquid. This transparency allows us to monitor the nanoparticle growth and formation, analyzing the change in color and also by mean of the UV-Vis spectra. The microemulsions were the chemical reactor for the reduction of Pd and Au.

5.1.1. Changes of color during each step of synthesis of Pd-Au NPs

During the synthesis of Pd-Au NPs, the change of color is a very important factor to take into consideration, because it allows us to check out if the reactions are proceeding. As the microemulsion is colorless and when H_2PdCl_4 was added to form the Pd NP, the color of the new solution changed to light yellow, see figure 3A. When hydrazine was added to this solution to reduce the palladium, a change of color from light yellow to light brown was observed, see figure 3B, according to the reported by Hosseinkhani et al.In the step when $HAuCl_4$ was added to the solution of Pd NPs to form the Pd-Au NPs, the change of color was more visible, from light brown to dark brown, see figure 3C. Finally, with the addition of hydrazine and dodecanethiol to this solution, a new change of color was observed, from dark brown to a purple brown, see figure 3D.

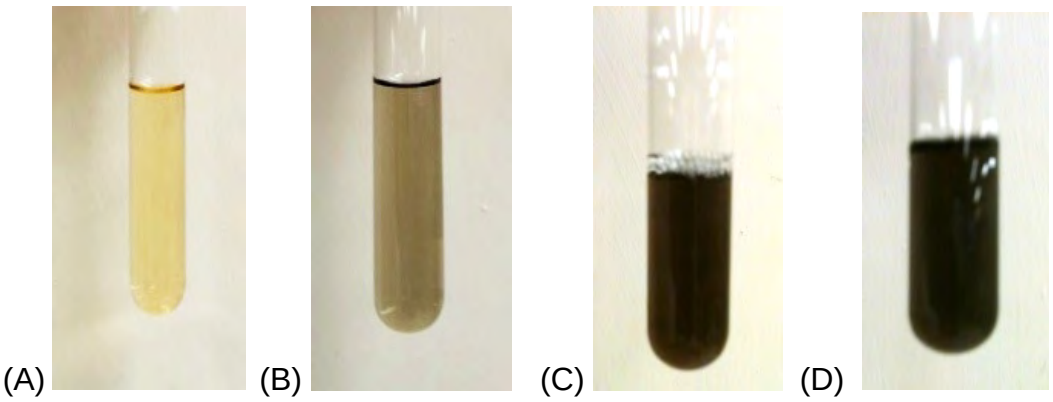

Figure 3. Color of (A) Microemulsion + H_2PdCl_4, (B) Microemulsion + H_2PdCl_4 + N_2H_4 (C) Solution of Pd NP + $HAuCl_4$ (D) Solution of bimetallic Pd-Au NP + N_2H_4 + $[CH_3(CH_2)_{11}SH]$

5.1.2 UV-Vis Spectroscopy

First of all, to determine the complete reduction of Pd and Au, some UV-Vis analysis were performed in order to measure the absorbance to a determined wavelength of the different samples prepared during this project. For the sample of AOT in isoctane, the UV-Vis spectrum does not show any absorption peak, as it can be seen in figure 4.

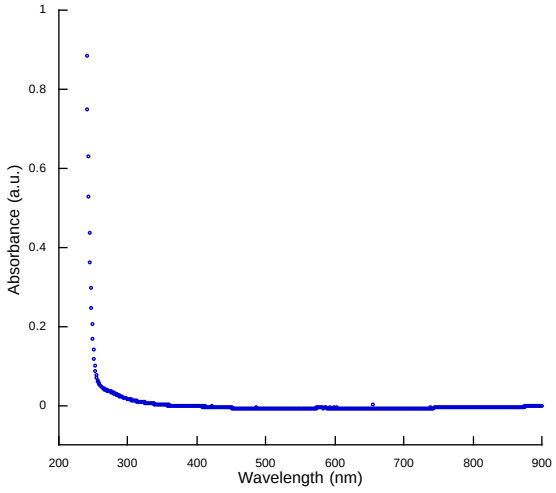

Figure 4. UV-Vis spectrum of AOT in isooctane system, [AOT]=0.1M. This spectrum does not show any absorption peak

For the sample of AOT in isoctane with added water, the so-called “microemulsion”, the UV-Vis spectrum does not show any absorption peak, as seen in figure 5. A similar study has been reported by Prasad et al., 1998.

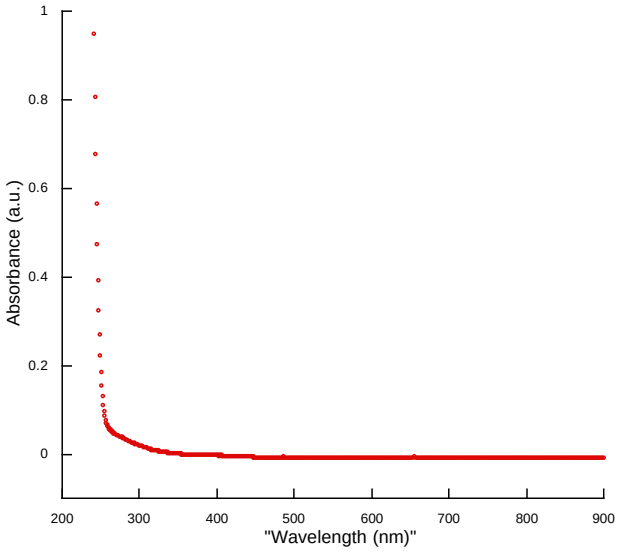

Figure 5. UV-Vis spectrum of the AOT-isooctane-water system, [AOT]=0.1M, [H_2O]=5[AOT]. This spectrum does not show any absoption peak.

For the sample of microemulsion with water and H_2PdCl_4, the spectrum shows a peak of absorption at around 230 nm (see Figure 6), wavelength characteristic or bare palladium NPs of sizes smaller than 10 nm (Henglein, 2000), and after 24 hours a peak of absorption appears at around 280 nm, wavelength characteristic and indicative of the growth and presence of Pd NPs, as it can be seen in figure 8.

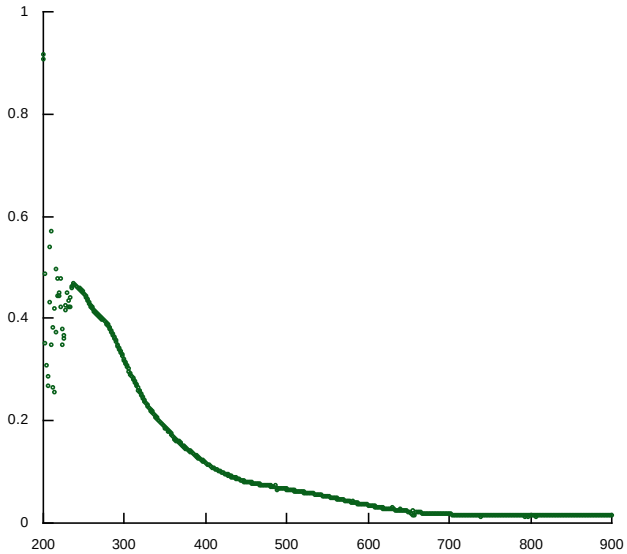

Figure 6. UV-Vis spectrum of the Pd NP. AOT-water/H_2PdCl_4-isooctane system, [AOT]=0.1M, [H_2PdCl_4]=1x10^{-4}M, W=5, [N_2H_4]=1 µL/ mL microemulsion. This spectrum shows an absorption peak at 280 nm

Finally, after 24 hours, it is possible to add $HAuCl_4$ and dodecanethiol to form the Pd-Au NP, which starts showing a shoulder at around 520 nm, wavelength expected for the SPRB of gold NP according to the study of Creighton et al., see figure 7. (Creighton et al., 1991).

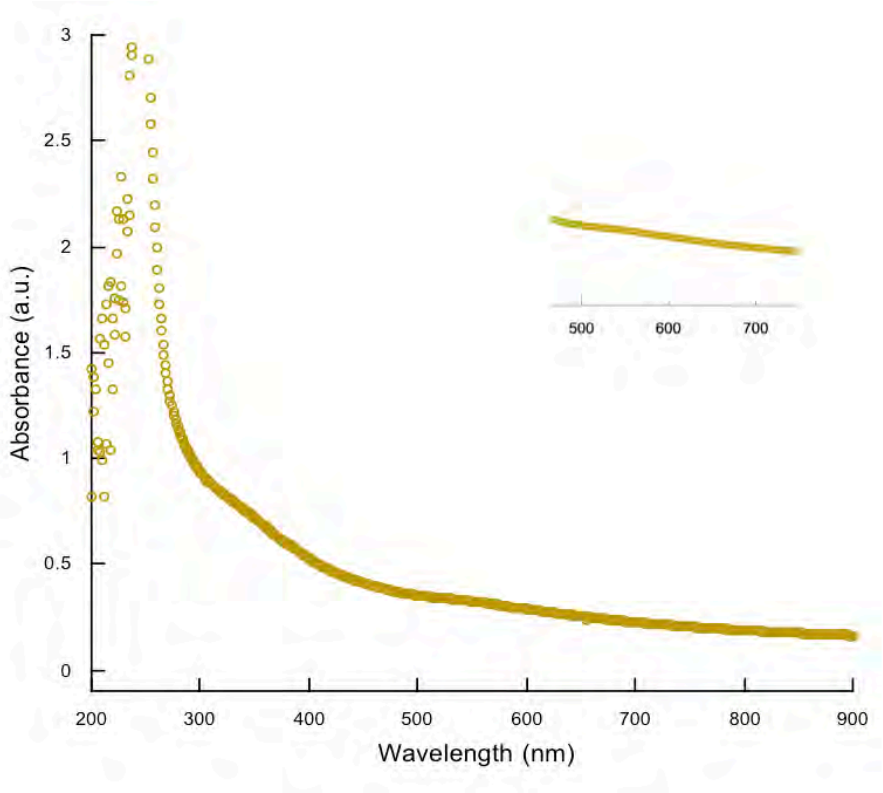

Figure 7. UV-Vis spectrum of bimetallic Pd-Au NP. AOT-water/ H_2PdCl_4-isooctane system, [AOT]=0.1M, $[H_2PdCl_4]=1x10^{-4}M$, W=5, $[N_2H_4]$=1 µL/ mL microemulsion, $[HAuCl_4]=2x10^{-4}M$, $[CH_3(CH_2)_{11}SH]$= 9µL/mL microemulsion. The curve displays a slight shoulder around 520 nm, value expected for gold NP.

To verify the formation of Pd and Pd-Au NPs, some UV-Vis analysis were performed in order to determine their behaviour throughout the time (8 days). In case of Pd NPs, every day that the sample was taken for analysis, around 1 hour after returning the sample to the system, it was observed a precipitated at the bottom of the reactor and some suspended solids in the solution. Before measuring the absorbance of the suspension, it was agitated in the mini vortexer VWR, because the system always showed a small precipitate at the bottom of the reactor, and even after agitation, the system got dispersed almost immediately. The spectra are shown in figure 8.

From this analysis, it can be noted that at a time of 24 hours, the NPs of palladium are already formed and ready for the next step of the synthesis by sequential reduction.

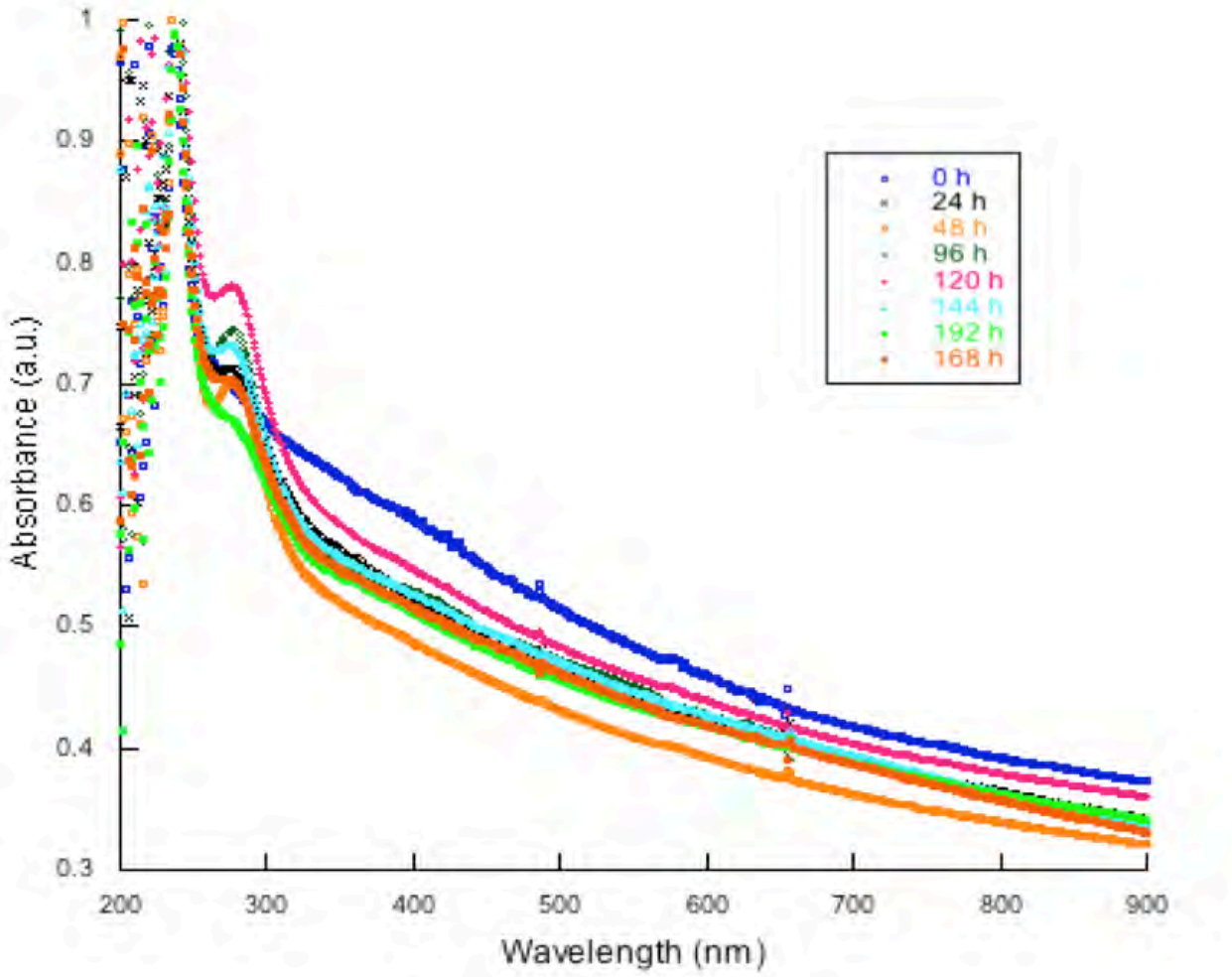

Figure 8. UV-Vis spectra of Pd NP at times of 24, 48, 96, 120, 144, 168 and 192 h. The curves shows the same wavelength of 280 nm but different absorbances throughout the time. AOT-water/ H_2PdCl_4-isooctane system, [AOT]=0.1M, $[H_2PdCl_4]=1x10^{-4}$M, W=5, $[N_2H_4]$=1 µL/ mL microemulsion.

The results obtained of the synthesis performed to analyze the behaviour of the passivated Pd-Au NP throughout the time (8 days) are shown in the spectra of figure 9. Every day the sample was taken for analysis, it was observed a precipitated at the bottom of the reactor and some suspended solids in the solution. Before measuring the absorbance of the solution, it was agitated in the mini vortexer VWR, because the system always showed a precipitate at the bottom of the reactor, and even after agitation, the system dispersed almost immediately.

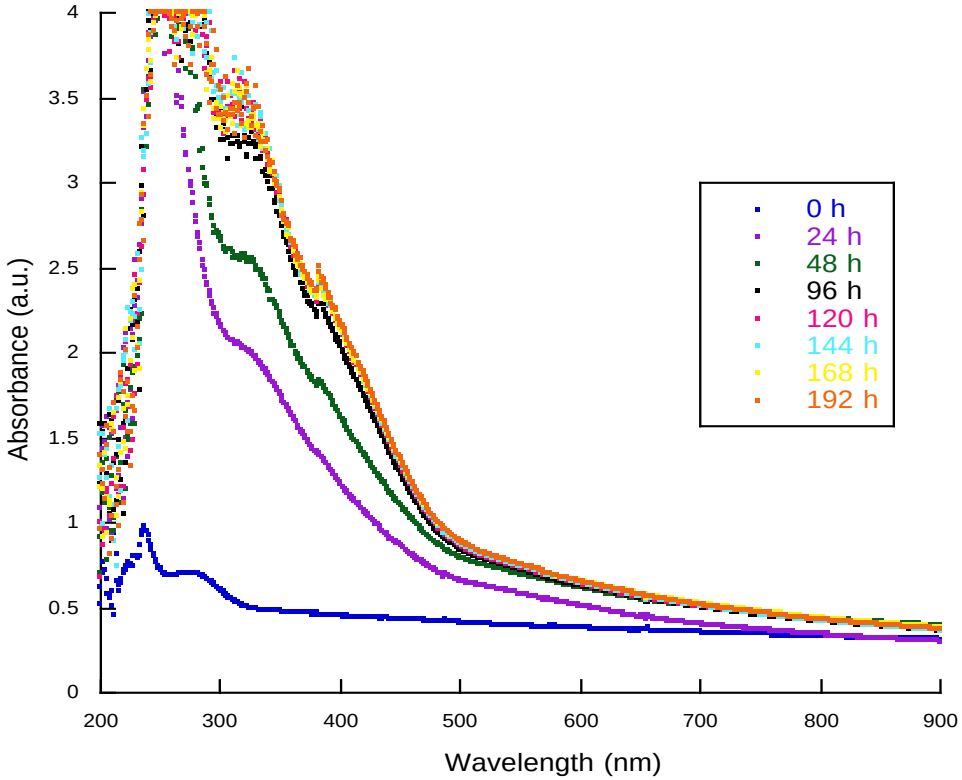

Figure 9. UV-Vis spectra of Pd-Au NP at times of 0, 24, 48, 96, 120, 144, 168 and 192 h. AOT-water/ H_2PdCl_4-isooctane system, [AOT]=0.1M, $[H_2PdCl_4]=1x10^{-4}M$, W=5, $[N_2H_4]$=1μL/mL microemulsion, $[HAuCl_4]= 2x10^{-4}M$, $[CH_3(CH_2)_{11}SH]$= 9μL/mL microemulsion.

In the table 1, it is shown a comparison of the wavelength and its absorbance in an experiment ran during 192 hours by the sequential reduction synthesis. The system presents a SPRB that goes from 279 nm (characteristic of pure Pd NP) until 384 nm which suggests the presence of an alloyed system of palladium and gold since the SPRB is in between the characteristic SPRB of pure Au (520 nm) and pure Pd (279 nm).

Table 1. Comparison of the wavelength and absorbance of Pd-Au NP through time

Time (h)	Wavelength (nm)	Absorbance (a.u.)
0	279	0.7
24	324	2.03
48	328	2.51
96	384	2.29
120	384	2.29
144	384	2.29
168	384	2.29
192	384	2.29

5.1.3 Characterization of Pd-Au nanoparticles: TEM and HRTEM studies

The bimetallic Pd-Au NP produced were measured and observed by TEM. As shown in TEM images, the Pd-Au bimetallic particles are aggregated. In order to stabilize a suspension of isolated, individual NP, its surface was covered with thiol molecule or dodecanethiol.

Two different TEM studies were performed:

In the first one, 20 µL of isooctane were used to wash the sample of passivated Pd-Au NP in the copper grid. In the figure 10, a representative TEM image of the surfactant stabilized bimetallic Pd-Au NP is shown. In this first study, the NP were low monodispersed and highly agglomerated.

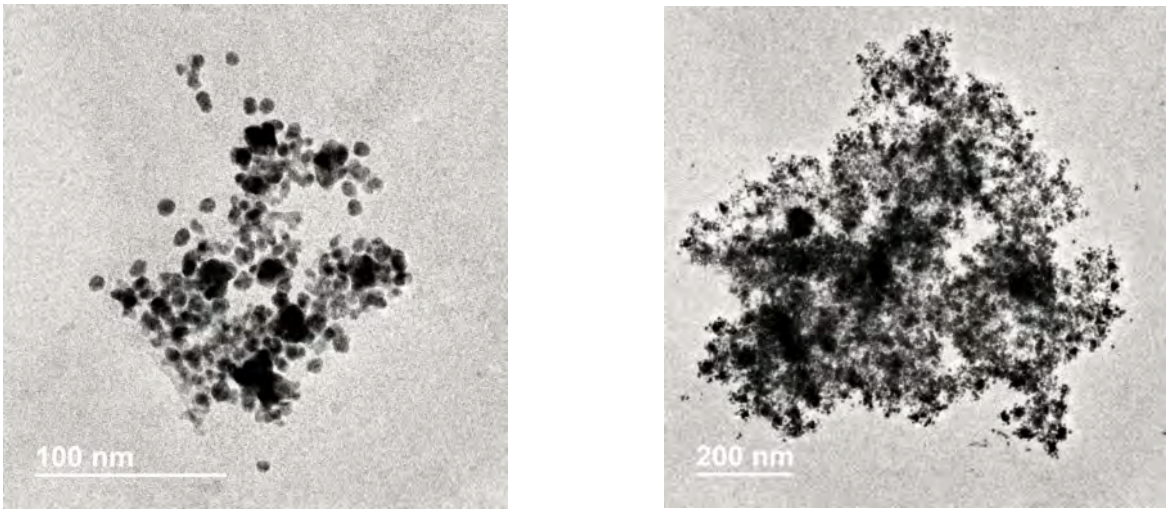

Figure 10. TEM images of bimetallic Pd-Au NP washed with 20 µL of isooctane. These NP were low monodispersed and highly agglomerated.

Due to the fact the NP could not been observed with good resolution, a second study was performed. In this study, the sample in the copper grid was washed with another 20 µL of isooctane to get a better resolution. In the figure 11, a representative TEM image of the surfactant stabilized, mono and bimetallic Pd-Au NP is shown. The NP obtained improved its monodispersity and were less agglomerated.

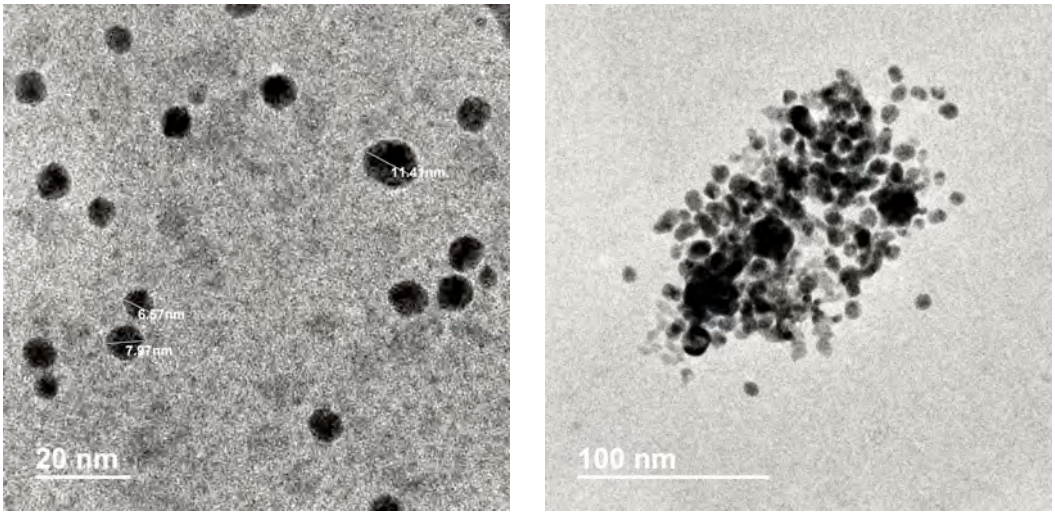

Figure 11. TEM images of bimetallic Pd-Au NP where the scale represents 20 and 100 nm. These NP showed a better monodispersity and were less aglomerated.

According to the results obtained to characterize the NP in HRTEM, it is very important to prepare the sample of Pd-Au NP with at least 40 µL of isooctane to avoid problems of agglomeration of the NPs which affects the correct analysis by either HRTEM or particle size distribution. This according to the experience acquired during this investigation for the characterization of NPs.

In the figure 12, a HRTEM image show the sizes of the NP synthesized.

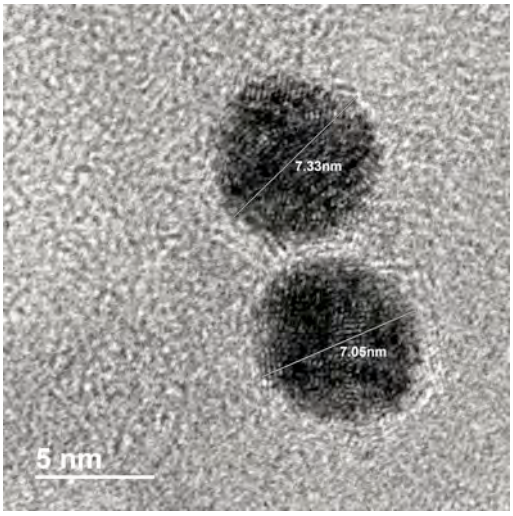

Figure 12. HRTEM image of a Pd-Au NP at a scale of 5 nm. The NP sizes are 7.05 and 7.33 nm, respectively.

In this synthesis, the HRTEM image of a Pd-Au NP synthesized by the sequential reduction method (figure 13) was analyzed to determine the crystallographic planes and its corresponding components. The information gotten is shown in figure 14, five crystallographic planes were found: (222) for AuPd (distance=1.132 Å), (022) for AuPd (distance=1.375 Å), (112) for Au_3Pd (distance=1.666 Å), (002) for AuPd (distance=2.000 Å) and (111) for AuPd (distance=2.276 Å), the structure crystallized for the compounds is cubic and space group: fm-3m. According to the planes observed, the nanoparticle is an alloyed AuPd bimetallic nanoparticle, (Data from ICSD: Inorganic Crystal Structure Database, Reference Code: AuPd: 98-005-8571 and Au_3Pd: 98-018-0872). These results are consistent with those of UV-Vis spectroscopy, see figure 9.

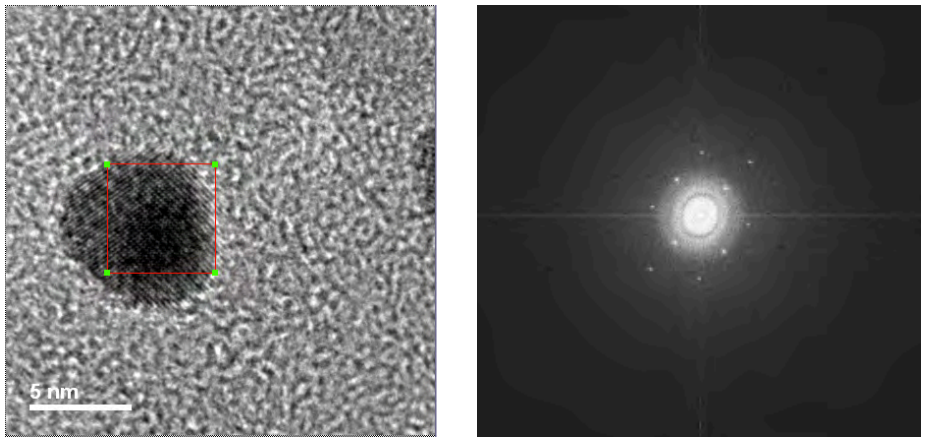

Figure 13. HRTEM image of a bimetallic Pd-Au nanoparticle. AOT-water/H_2PdCl_4-isooctane system, [AOT]=0.1M, [H_2PdCl_4]=1x10^{-4}M, W=5, [N_2H_4]=1µL/mL microemulsion, [$HAuCl_4$]= 2x10^{-4}M, [$CH_3(CH_2)_{11}SH$]= 9µL/mL microemulsion.

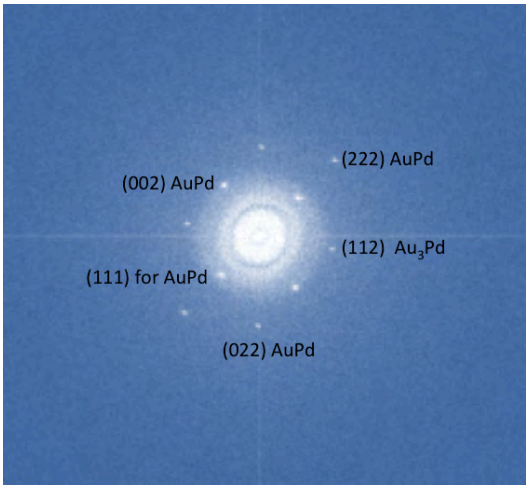

Figure 14. Diffractogram of the crystallographic planes for the nanoparticle Pd-Au. These are: Planes (002), (022), (111) and (222) for AuPd and plane (112) for Au_3Pd.

5.1.4 Particle Size Distribution

The results of this synthesis were also used to obtain the particle size distribution of 200 bimetallic Pd-Au NP. The results are shown in the following histogram (figure 15).

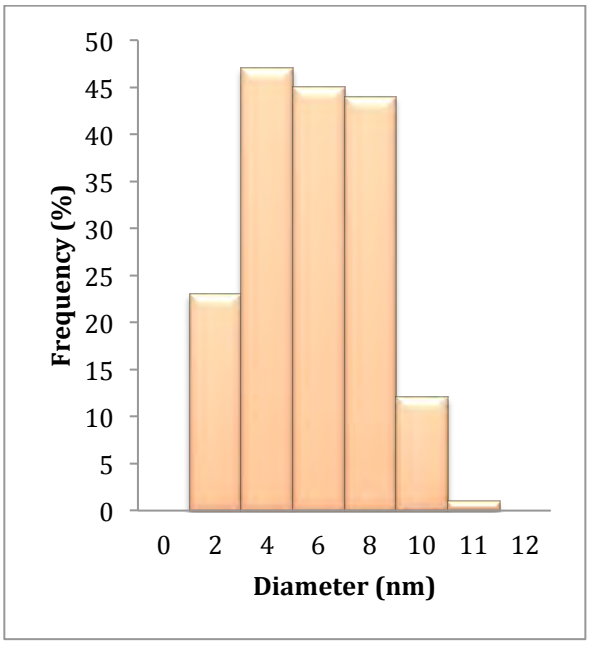

Figure 15. Particle size distribution of Pd-Au NP prepared by the sequential reduction method, measured from 200 particles in TEM images using the ImageJ program.

The NP average size is 5.70 ± 2.18 nm with a variation coefficient of 0.38, and a polidispersity of 38.22%.

5.1.5 EDX Results for Pd and Pd-Au nanoparticles

EDX analysis was performed to Pd NPs and the result shows a nanoparticle composition of 89.06 % of Pd, 10.06 % of S and 0.88% of Na (figure 16).

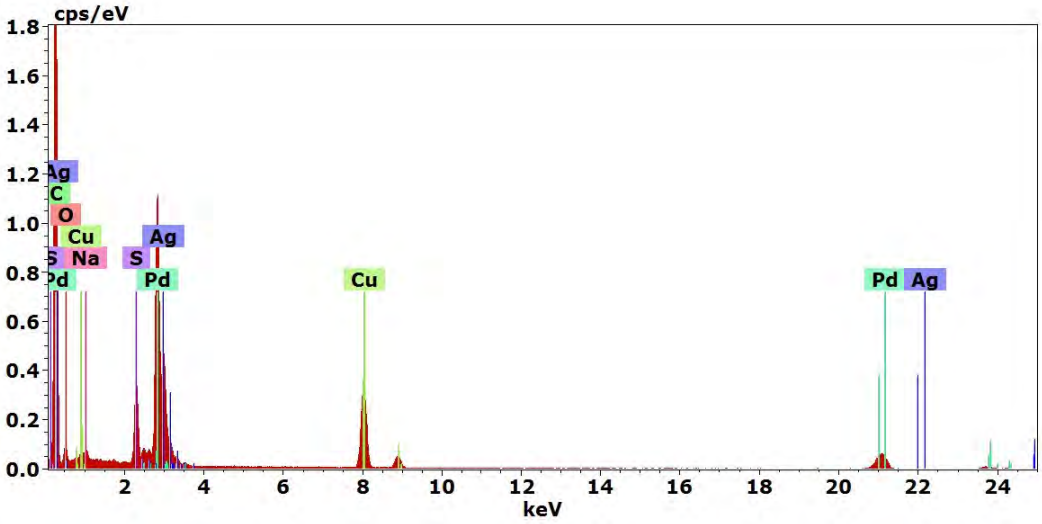

Figure 16. EDX elemental analysis by line scan across a Pd nanoparticle. AOT-water/ H_2PdCl_4-isooctane system, [AOT]=0.1M, $[H_2PdCl_4]=1x10^{-4}$M, W=5, $[N_2H_4]$=1 µL/ mL microemulsion.

EDX analysis was performed to Pd-Au NP prepared by the sequential reduction method and the result shows a nanoparticle composition of 76.37 % of Au , 7.77 % of Pd and 14.86 % of S (figure 17). The Na and S appear because are part of the AOT molecule and the –SH group of dodecanethiol.

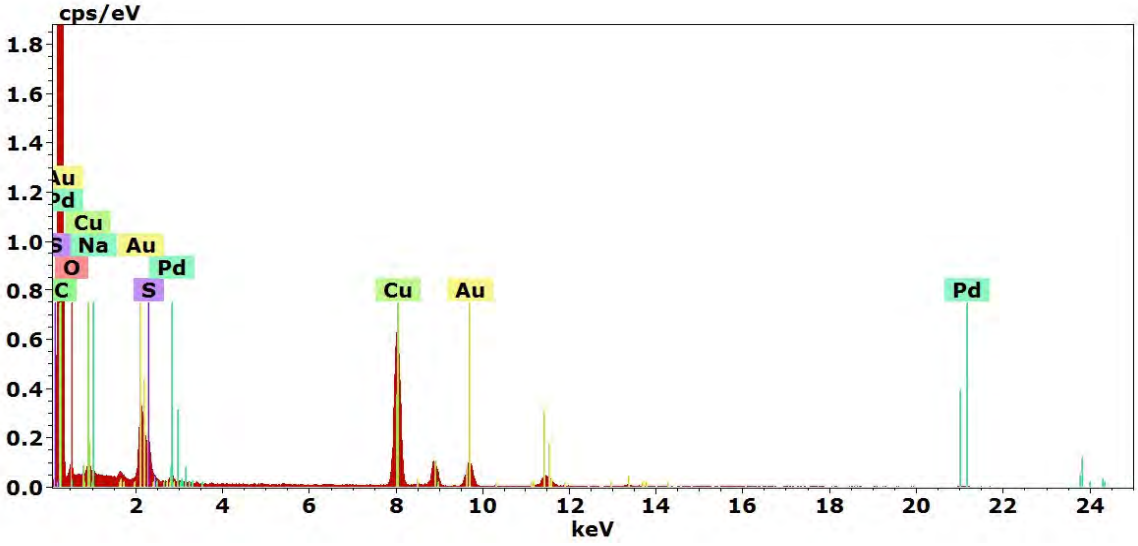

Figure 17. EDX elemental analysis by line scan across a bimetallic Pd-Au nanoparticle. AOT-water/ H_2PdCl_4-isooctane system, [AOT]=0.1M, $[H_2PdCl_4]=1x10^{-4}$M, W=5, $[N_2H_4]$=1 µL/ mL microemulsion, $[HAuCl_4]= 2x10^{-4}$M, $[CH_3(CH_2)_{11}SH]$= 9µL/mL microemulsion.

5.2. Simultaneous reduction of Pd and Au for synthesis of Pd-Au NPs

5.2.1 Characterization of Pd-Au nanoparticles: TEM and HRTEM studies

The simultaneous reduction of Au and Pd for synthesis of Pd-Au NPs was studied, to determine the crystallographic planes of the NPs and also to obtain their particle size distribution, the results were analyzed with Digital Micrograph® 3.7.0. In the figure 18, it is shown the procedure to determine the distances of the corresponding NPs crystallographic planes.

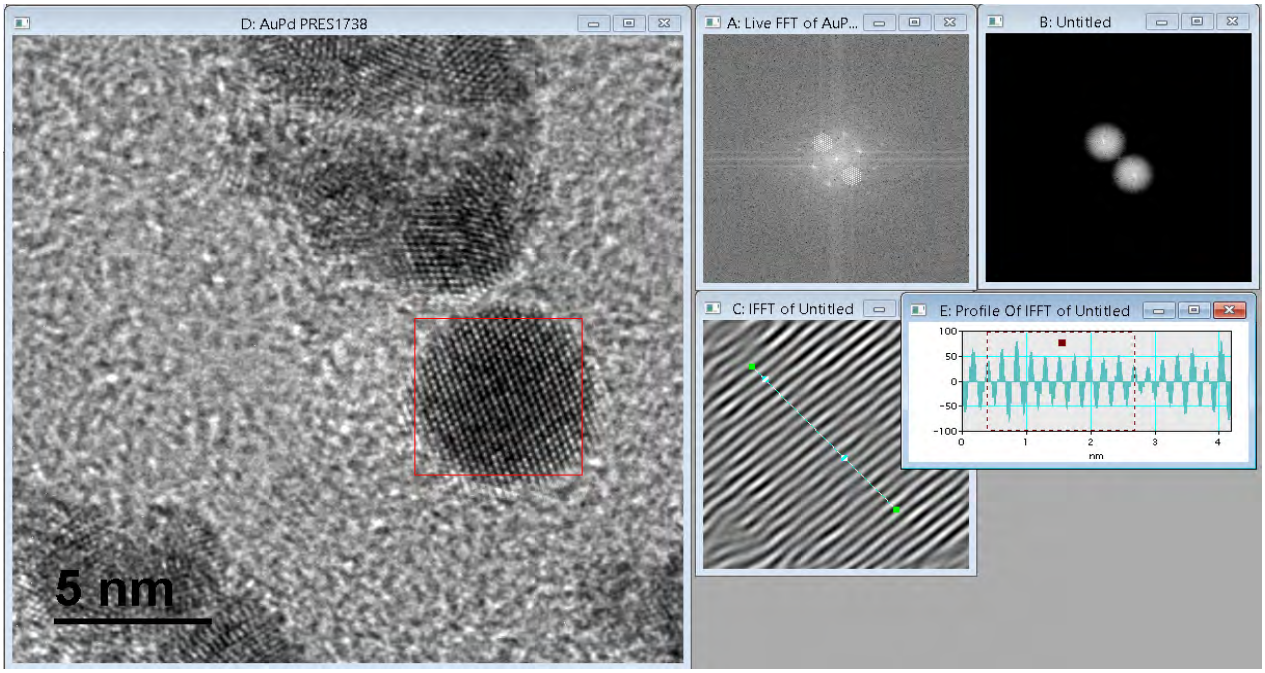

Figure 18. Determination of the crystallographic structure of Pd-Au NPs prepared by the simultaneous reduction method. These were synthesized in a 0.1 M microemulsion of AOT-water-isooctane with $HAuCl_4$:H_2PdCl_4 1:1.

The measured distances for the inner layer and their corresponding crystallographic planes were d_1=2.28 Å, d_2=2.282 Å, (111) for $AuPd_3$ and d_3=2.324 Å, (111) for AuPd. The measured distances for the outer layer and their corresponding crystallographic planes were d_1=1.057 Å, d_2=1.162 Å, (222) for AuPd and d_3=1.225 Å, (311) for Au. See figure 19. The structure crystallized for the compounds is cubic with space group Fm-3m (Reference codes: For AuPd: 98-005-8571, for $AuPd_3$: 98-018-0876).

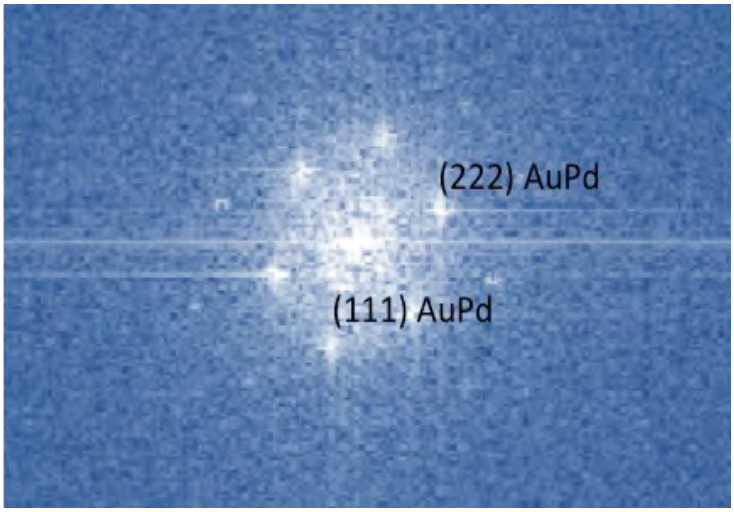

Figure 19. Diffractogram obtained from the FFT of the crystallographic planes for a Au-Pd NP prepared by the simultaneous reduction method. These correspond to AuPd: d_{111}=2.324 Å and d_{222}=1.162 Å.

The figure 20 shows a nanoparticle that was analyzed and the results obtained turned out that the distances measured 2.364 Å and 2.055 Å nearly corresponds to the crystallographic planes (111) and (002) of Au_3Pd. The structure crystallized for the compounds is cubic, space group: Pm-3m.

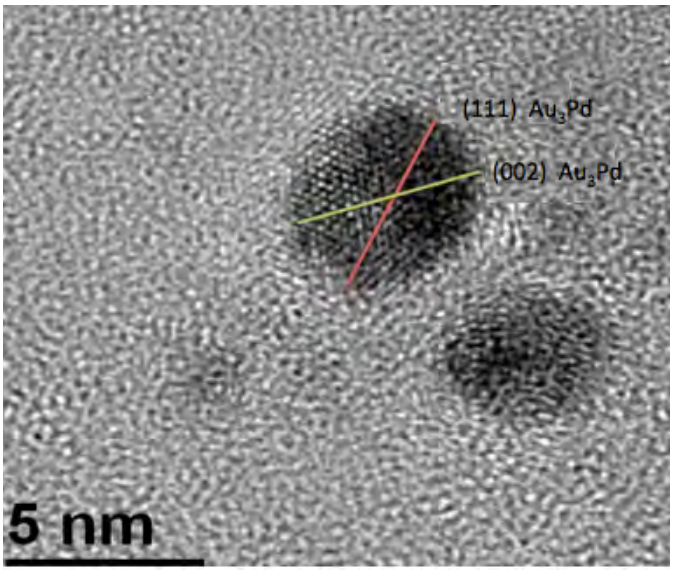

Figure 20. Electronic micrograph for the crystallographic planes for a Pd-Au NP. These correspond to Au_3Pd: d_{111}=2.364 Å and d_{002}=2.055 Å.

5.2.2 Particle Size Distribution

The results of this synthesis were also used to obtain the particle size distribution of 575 Pd-Au NP as those seen in the figure 21. The results are shown in the histogram of figure 22.

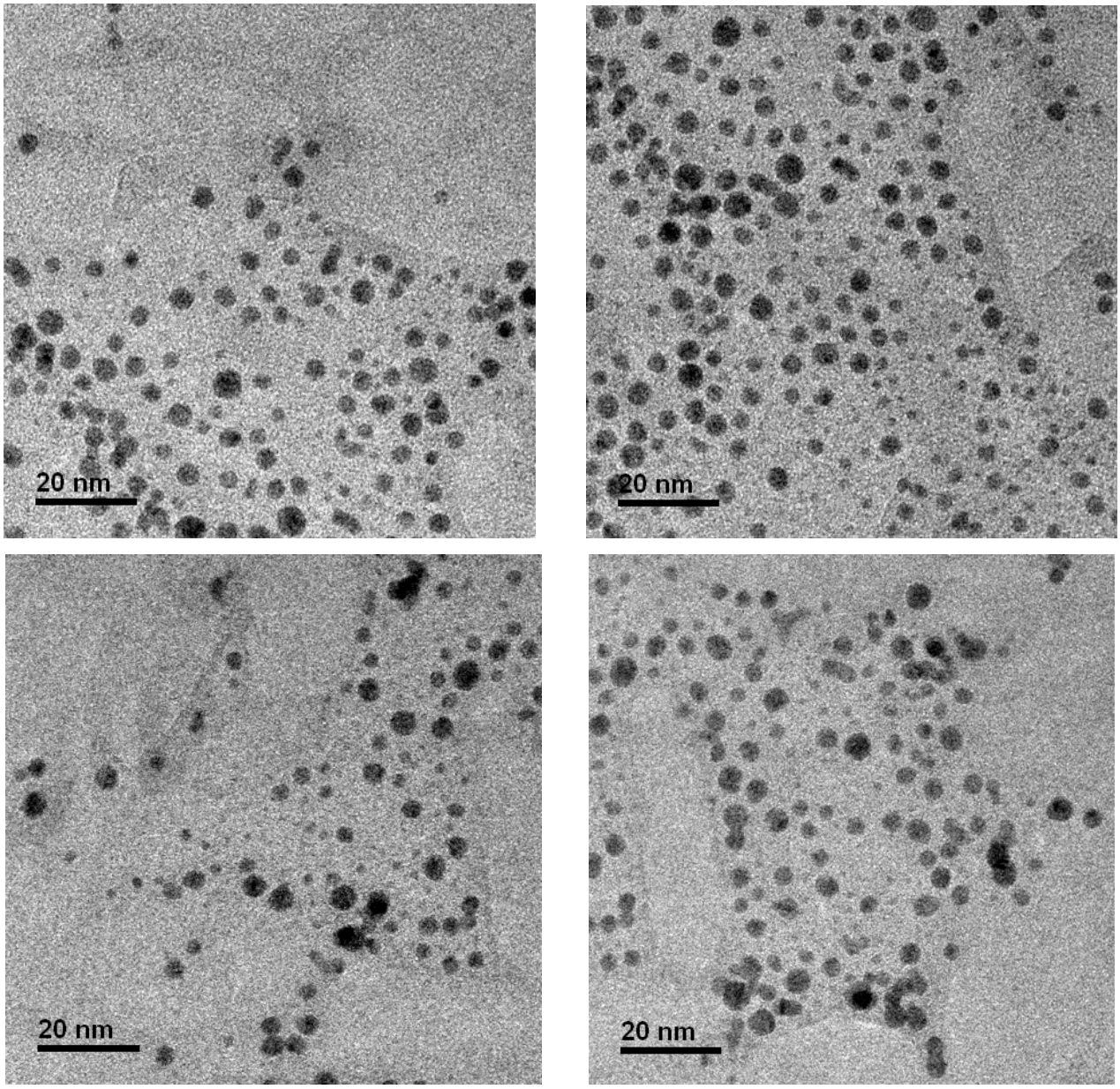

Figure 21. TEM micrographs for Pd-Au NP synthesized by simultaneous reduction and washed twice with 20 µL of isooctane. NP average size of 3.6 ± 1.1 nm, and 33% of polidispersity.

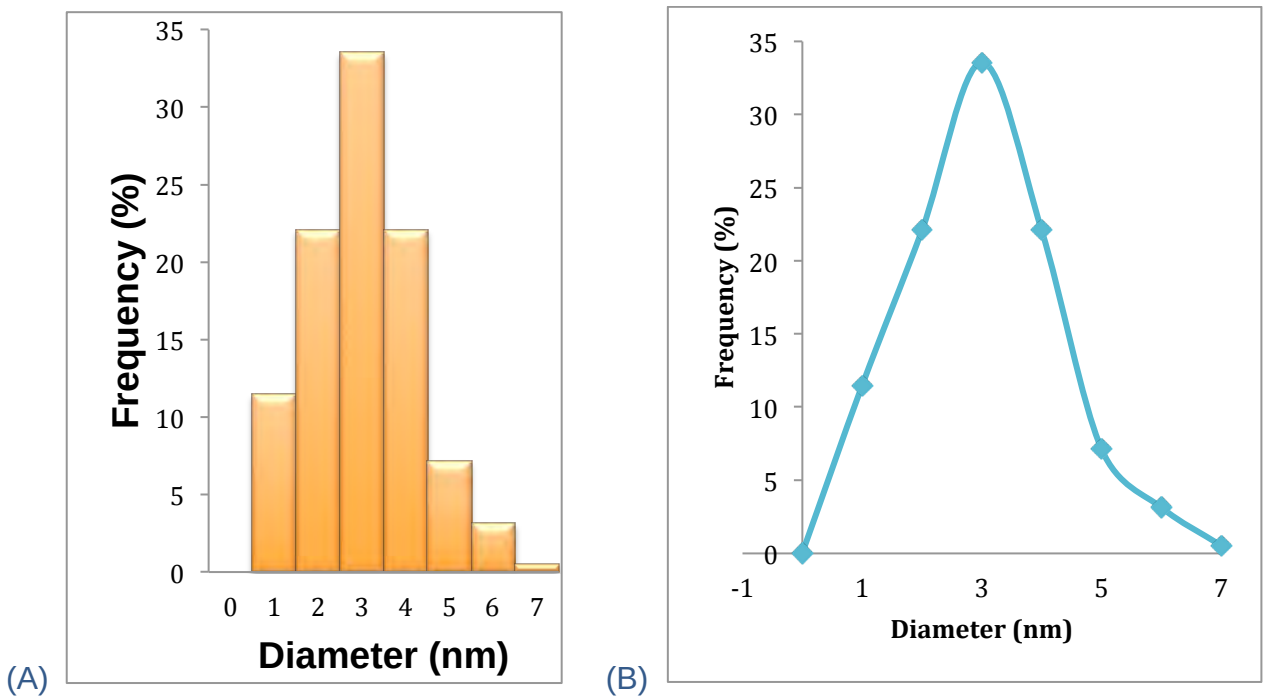

Figure 22. (A) Particle size distribution of bimetallic Pd–Au NP synthesized by the simultaneous reduction method and measured from 575 particles in TEM images. (B) NP average size.

The NP average size is 3.57 ± 1.18 nm with a variation coefficient of 0.33 and a polidispersity of 33.04%.

5.2.3 STEM HAADF and EDX Analysis

Some samples synthesized by the simultaneous reduction method were sent to CNMN-IPN to characterize them and complement the results initially obtained in our experiments, using there the Atomic Resolution Analytical Microscope, JEM ARM 200F to analyze the NPs samples. The results are shown below.

5.2.4 STEM-HAADF and EDX Results

Figure 23 shows the STEM-HAADF image of a Pd-Au NP. 23A shows that in the nanoparticle analyzed there are two elements, one brighter than the other; according to the contrast, the brighter one corresponds to gold (Z=79) and the less brighter corresponds to palladium (Z=46). The EDX spectrum of the NP can be seen in figure 24. A deeper analysis of this NP can be done with a linescan of it as shown in figure 23B, which results can be seen in figure 25 and 26. From the graph of figure 26, it can be concluded that gold is mostly in the center of the NP and that palladium is in its sourroundings.

(A)

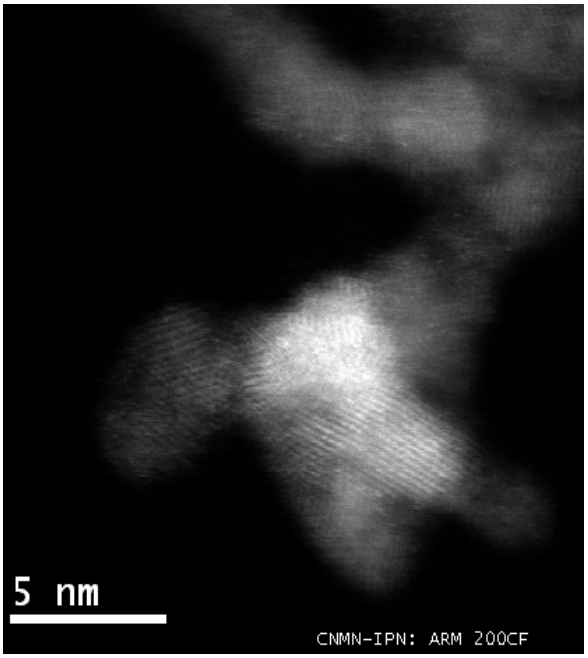

(B)

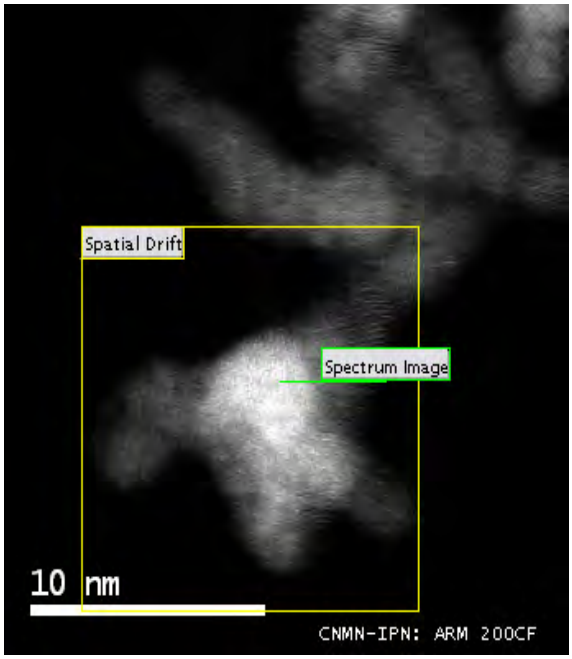

Figure 23. (A) STEM-HAADF image of a bimetallic Pd-Au NP,
(B) STEM-HAADF linescan of a bimetallic Pd-Au NP synthesized by simultaneous reduction method.

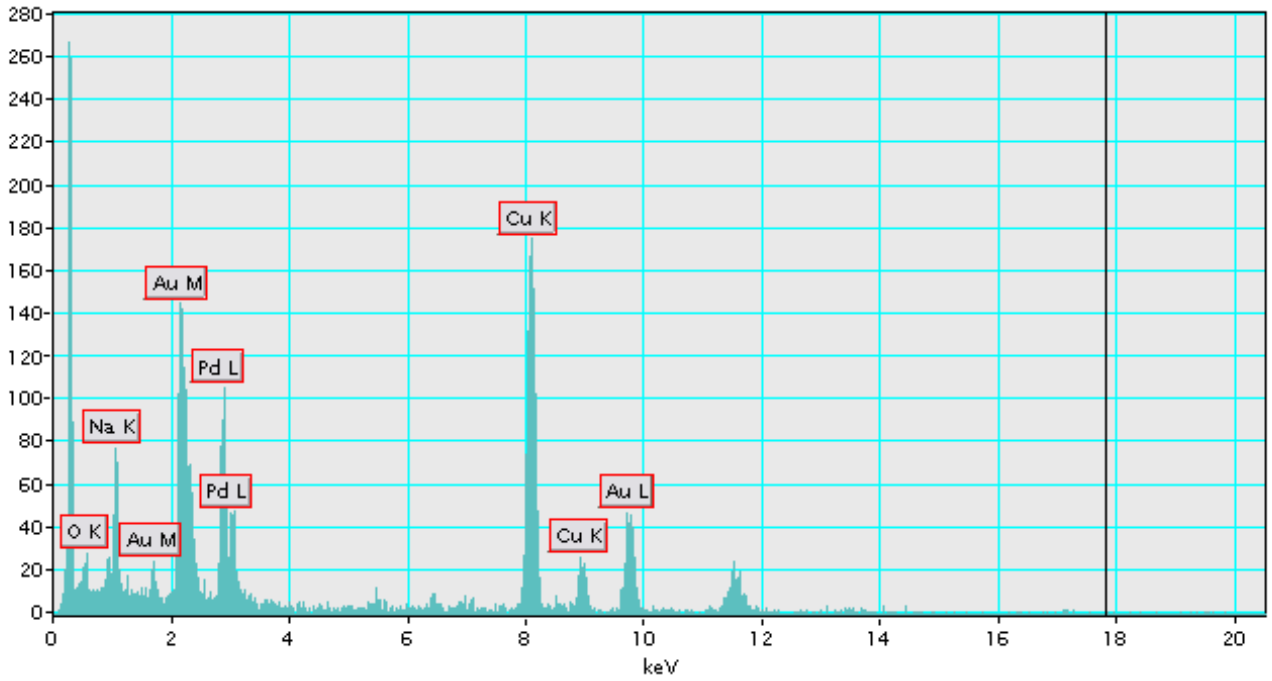

Figure 24. EDX elemental analysis for Pd-Au NPs synthesized by simultaneous reduction method in a 0.1 M microemulsion of AOT-water-isooctane with $HAuCl_4$:H_2PdCl_4 1:1

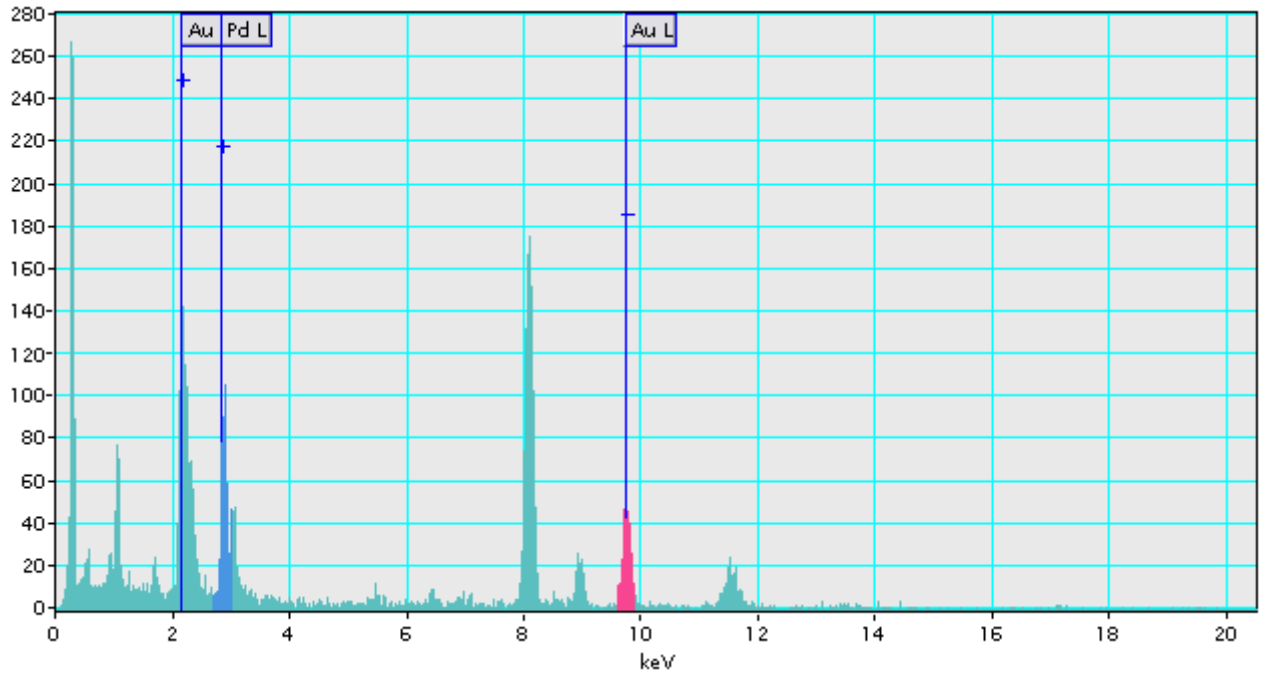

Figure 25. EDX elemental analysis of a Pd-Au nanoparticle, with Au and Pd electrons in L shell and Au electrons in M shell. AuPd nanoparticle from the synthesis in a 0.1 M microemulsion of AOT-water-isooctane with $HAuCl_4$:H_2PdCl_4 1:1.

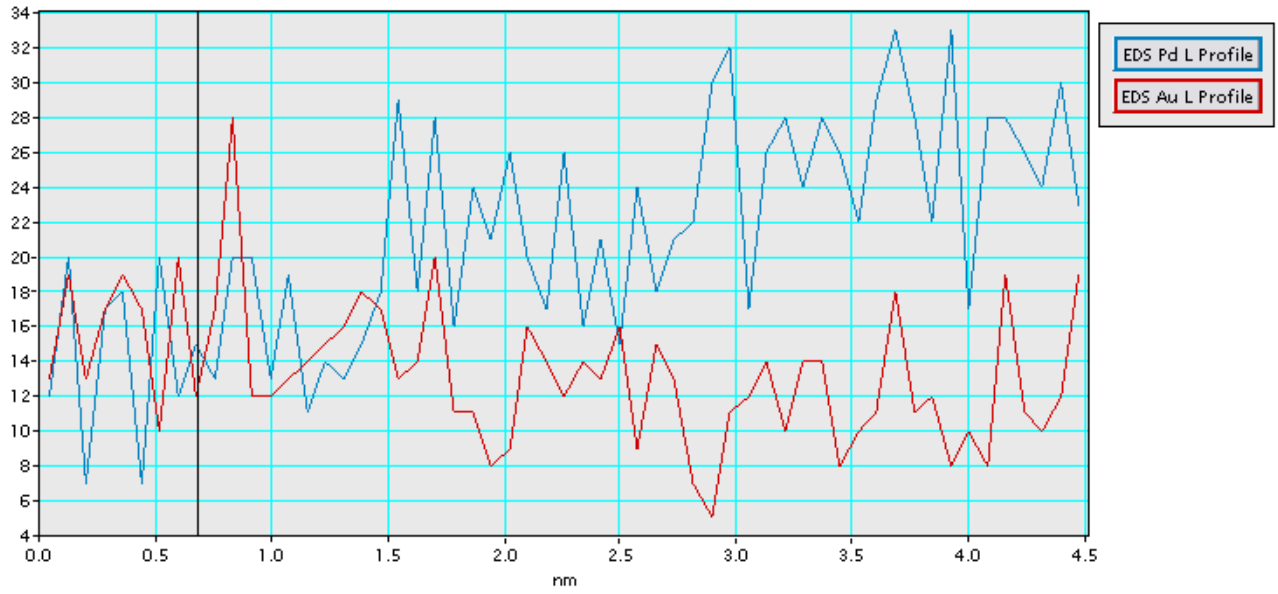

Figure 26. Line spectrum of a Pd-Au nanoparticle, with Au and Pd electrons in L shell.

The results of the analysis of the Pd-Au NP seen in figure 27 shows that according to the EDX line spectrum of figure 29, the nanoparticle is formed mostly for gold in its core and palladium covering it in a relatively constant proportion in the particle. This can be supported

with a EDX mapping of the elements Au and Pd, as seen in Figure 30 (A), (B) y (C). This clearly indicates that gold and palladium are well dispersed in the Pd-Au composite, but a little more gold in the core.

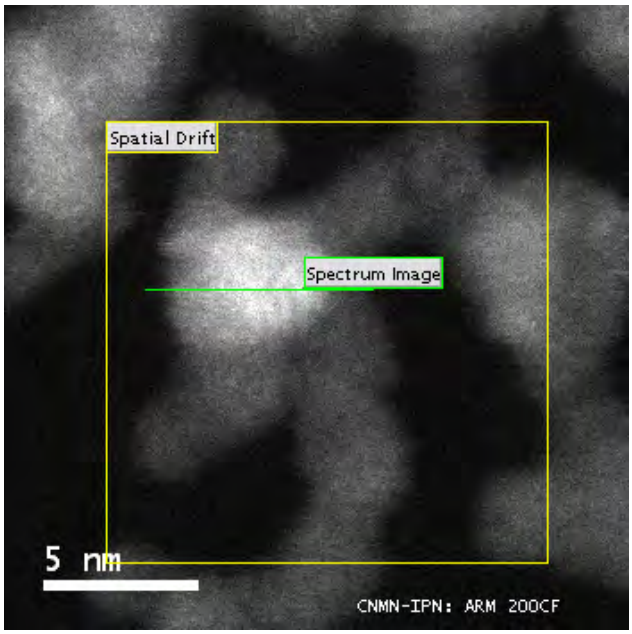

Figure 27. STEM-HAADF linescan of a bimetallic Pd-Au nanoparticle.

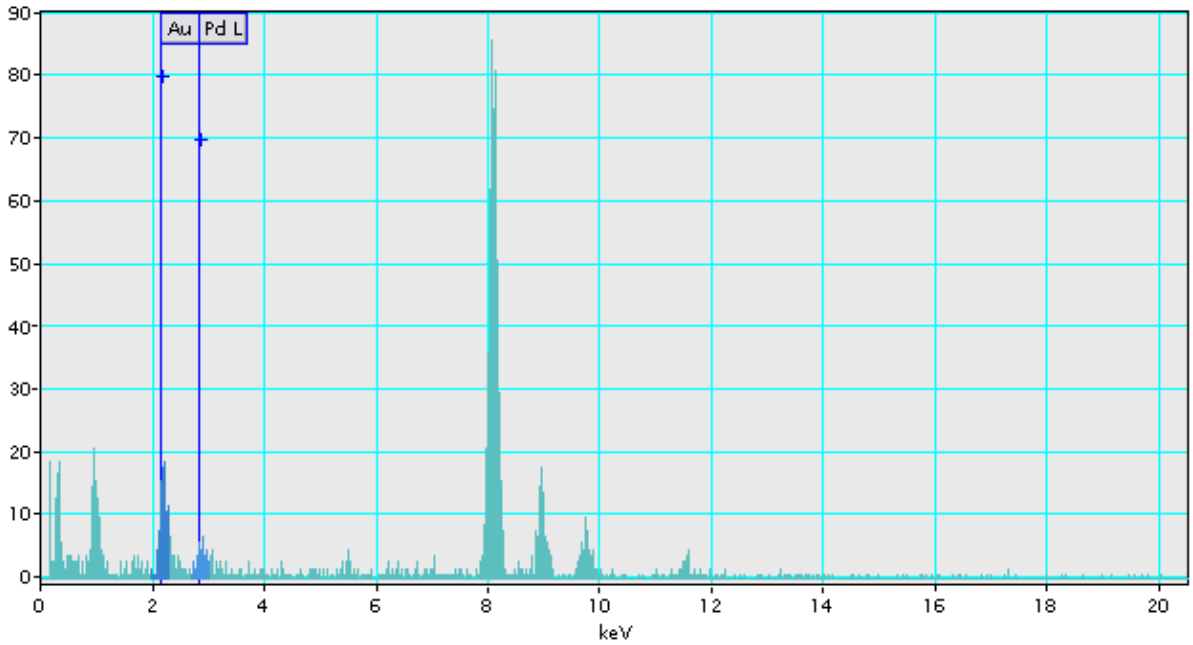

Figure 28. EDX elemental analysis of a Pd-Au nanoparticle, with Au and Pd electrons in L shell.

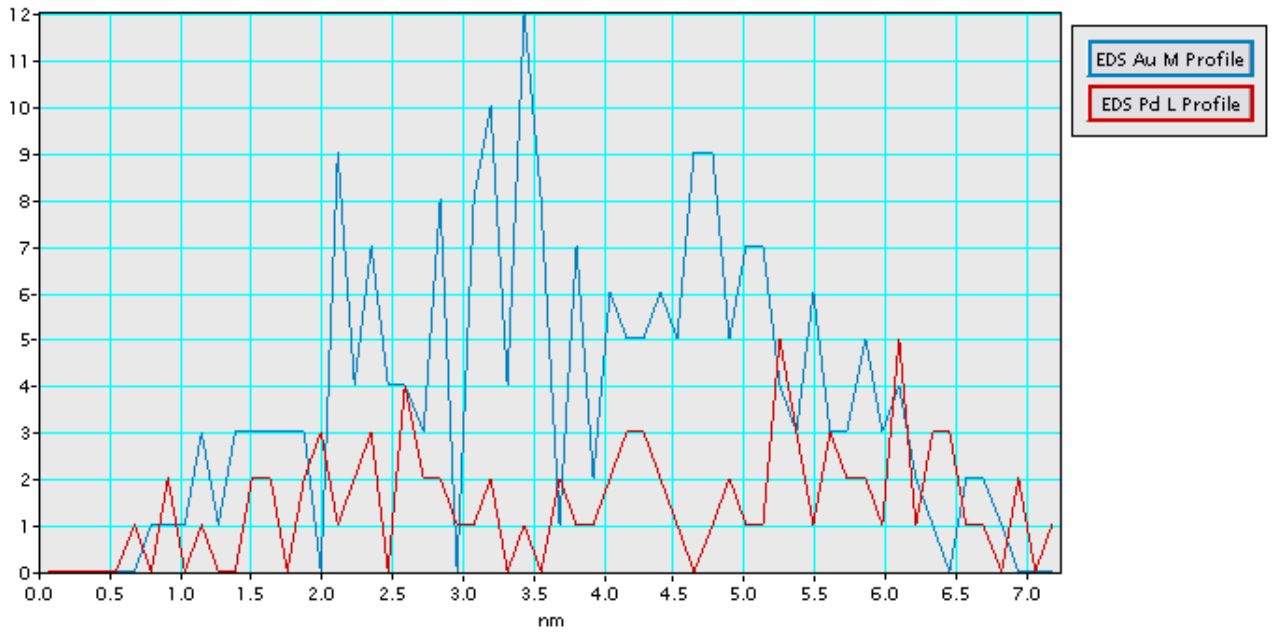

Figure 29. Line spectrum of a Pd-Au nanoparticle, with Au and Pd electrons in L shell.

(A) (B) (C)

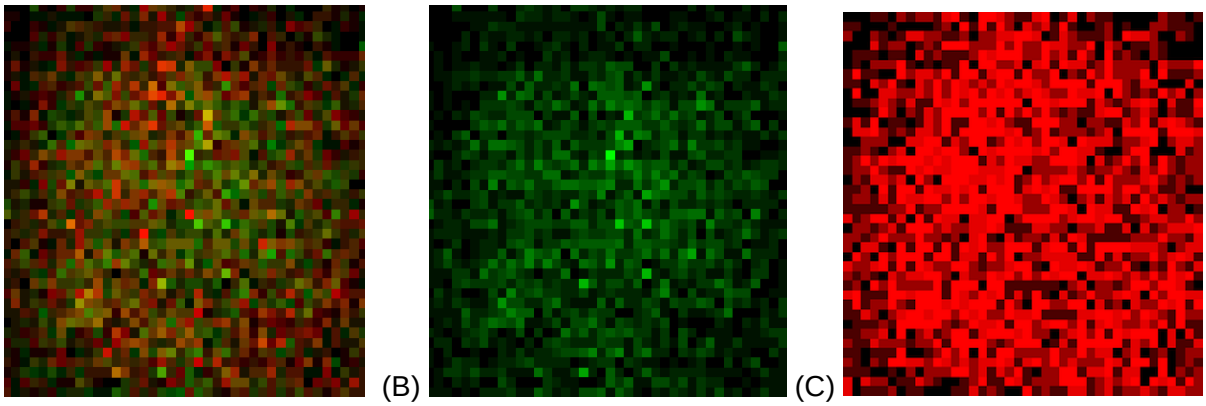

Figure 30. EDX mapping of (A) Pd-Au composite, (B) gold and (C) palladium

Another analysis of Pd-Au NP prepared by sequential reduction synthesis, (figure 31) shows that according to the EDX mapping of the elements Au and Pd, seen in figure 32 (A), (B) y (C) clearly indicates that gold and palladium are well dispersed in the Pd-Au alloyed system.

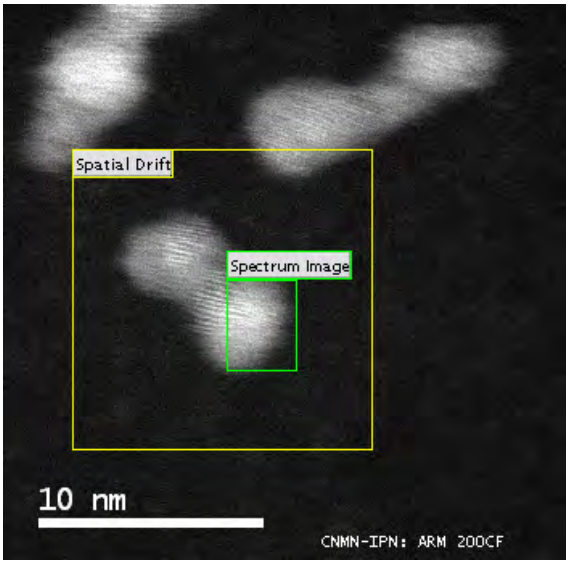

Figure 31. STEM-HAADF image of a bimetallic Pd-Au nanoparticle.

(A) 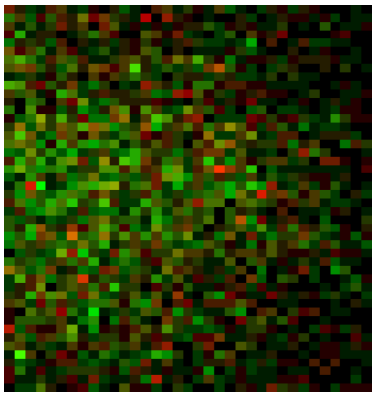 (B) 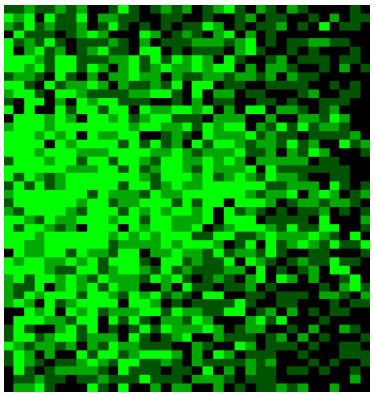 (C) 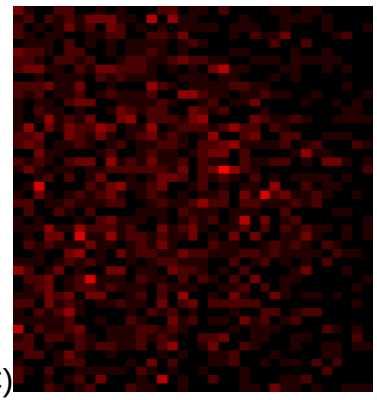

Figure 32. EDX mapping of (A) Pd-Au composite, (B) gold and (C) palladium

5.3 Insights from results obtained of the sequential and simultaneous synthesis method of Pd-Au NPs

With the sequential synthesis method of Pd-Au NPs it can be noticed that alloyed NPs are less well dispersed than those prepared by the simultaneous method.

The average particle size of these Pd-Au NP is smaller in the NP prepared by the simultaneous method. An explanation about particle size can be understood by the studies of Wu et al., in this investigation on particle size suggested that mosf ot he $AuCl_4^-$ and $PdCl_4^{2-}$ ions were reduced before the formation of the nuclei and the nuclei for the formation of Pd-Au bimetallic NP might be composed of Au and Pd atoms. The formation process of Pd-Au bimetallic NP could be described as a process in which first, most of the $PdCl_4^{2-}$ ions were reduced in a very short time. Pd atoms started to aggregate to form the nuclei and all the nuclei might be formed almost in less than 24 hours. When added the $AuCl_4^-$ ions, the palladium has acted as a catalyst and the ions were reduced in a very short time too, less than an hour, and Pd nuclei NP started forming again and since the nucleation rate of Au was much faster than that of Pd, the nuclei of the bimetallic system should be formed by the initiation of Au atoms and the composition of the nuclei might have higher Au content than that of the feeding solution. Then Au and Pd atoms codeposited onto the nuclei and grew to their final sizes. The faster deposition rate of Au than Pd led to the enrichment of Pd in the outer part of Pd-Au bimetallic NP.

The reduction potentials of Au and Pd are shown below:

$$AuCl_4^- + 3\,e^- \text{----> } Au + 4Cl^- \qquad 1.00V$$

$$PdCl_4^{2-} + 2\,e^- \text{----> } Pd + 4Cl^- \qquad 0.63V$$

Chapter 6. Conclusions

Bimetallic Pd-Au NPs were synthesized by sequential and simultaneous reduction of H_2PdCl_4 and $HAuCl_4$ in the presence of hydrazine, in the possible chemical compound form of AuPd, $AuPd_3$ or Au_3Pd.

The different synthesis performed during this thesis confirm that it is possible to synthesize Pd NPs and to reduce Pd and Au sequential and simultaneously in the aqueous domains of the AOT-isooctane-water microemulsions to form bimetallic alloyed Pd-Au NP.

The UV-Vis spectroscopy and HRTEM studies have shown also the formation of spherical alloyed Pd-Au NPs:

- The Pd-Au NPs synthesized by sequential reduction of Pd and Au has an average size of 5.70 ± 2.18 nm with a variation coefficient of 0.38, and a polidispersity of 38.22%.

- The Pd-Au NPs synthesized by simultaneous reduction of Pd and Au has an average size of 3.57 ± 1.18 nm with a variation coefficient of 0.33 and a polidispersity of 33.04%.

From the UV-Vis spectroscopy experiments it is shown that Pd and Au NP were produced, also alloyed Pd-Au NP. The SPRB for palladium is 280 nm, predominating in the passivated alloyed nanoparticle. In case of gold, the SPRB is 520 nm.

EDX elemental analysis performed to Pd-Au NPs prepared by sequential reduction and the result showed a nanoparticle composition of 76.37% of Au and 7.77% of Pd.

STEM-HAADF and EDX analysis of Pd-Au NPs prepared by the simultaneous reduction method suggest the formation of Pd-Au alloyed bimetallic NP, where gold and palladium are well dispersed in the NP and sometimes more gold or palladium can be found in the core of the NP.

Chapter 7. Recommendations and further research

There are some investigations that can be carried out concerning synthesis and applications of bimetallic Pd-Au NP in catalysis and environment.

In the aspects of applications of Pd-Au catalysts in the environment, there are some interesting studies which can be implemented, for example:

- For dechlorination of environmental contaminants, the study made by De Corte S. Hennebel et al. would be good, following the criteria used in their research entitled “Biosupported bimetallic Au-Pd nanocatalysts for dechlorination of environmental contaminants”.

- For alcohol oxidation reactions, the investigation of Aimee Mclennan in 2012, entitled: “Investigation of Au, Pd, and AuPd nanoparticle catalysts for alcohol oxidation reactions”, would be very helpful.

List of References

Aarts J. F. M., Phelan K. G. (1989). *Dehalogenation of fluorobenzene and chlorobenzene on Pd(111) studied by electron-energy loss spec- troscopy*. Surf. Sci., 222 (2_3), L853–L860.

Arbain, R.; Othman, M. & Palaniandy, S. (2011). *Preparation of iron oxide nanoparticles by mechanical milling*. Minerals Engineering, Vol.24, pp. 1-9

Bonarowska M., Burda B., Juszczyka W., Pielaszek J., Kowalczyk Z., Karpinski Z. (2001). *Hydrodechlorination of CCl_2F_2 (CFC-12) over Pd-Au/C catalysts*. Appl. Catal. B, 35 (1), 13–20.

Bönnemann, H. & Richards, R.M. (2001). *Nanoscopic Metal Particles - Synthetic Methods and Potential Applications*, Eur. J. Inorg. Chem. 245522480

Boutonnet, M.; Kizling, J.; Stenius, P. & Maire, G. (1982). *The Preparation of monodisperse colloidal metal particles from microemulsions*. Colloids Surf., Vol.5, pp. 209–225

Brown K.R., Walter D.G. & Natan M.J. (2000). *Seeding of colloidal Au nanoparticle solutions 2. Improved control of particle size & shape*. Chem. Mater. 12, 306–313.

Burda C., Chen X., Narayanan R. And El-Sayed M.A. (2005). *Chemistry and Properties of Nanocrystals of Different Shapes*. *Chem. Rev.*, 105(4): p. 1025

Cao G. (2004). *Nanostructures & Nanomaterials: Synthesis, Properties & Applications*. Editor, Imperial College Press, London, pp. 433.

Chen, D.H., Yeh, J.J. & Huang, T.C. (1999). *Synthesis of Platinum Ultrafine Particles in AOT Reverse Micelles*. Journal of Colloid and Interface Science, Vol.215, pp. 159–166

Chen M. S., Kumar D., Yi C., W. & Goodman D. W. (2005).*The promotional effect of gold in catalysis by palladium–gold*. *Science* 310, 291–293

Chen Y., Wang H., Liu Ch. et al., (2012). *Formation of monometallic Au and Pd and bimetallic Au–Pd nanoparticles confined in mesopores via Ar glow-discharge plasma reduction and their catalytic applications in aerobic oxidation of benzyl alcohol*. Journal of Catalysis, 289, 105–117.

Coker V. S., Bennett J. A., Telling N. D., Henkel T., Charnock J. M., Van der Laan G., Pattrick R. A. D., Pearce C. I., Cutting R. S., Shannon I. J., Wood J., Arenholz E., Lyon I. C., Lloyd J. R. (2010). *Microbial engineering of nanoheterostructures: biological synthesis of a magnetically recoverable palladium nanocatalyst*. ACS Nano, 4 (5), 2577–2584.

Cookson N.J. (2010). *Preparation and characterisation of bimetallic core-shell nanoparticles*, M.Res. thesis, University of Birmingham.

Coq B., Figueras F. (2001). *Bimetallic palladiumcatalysts:influenceof the co-metal on the catalyst performance*. J. Mol. Catal A: Chem., 173 (1_2), 117–134.

Creighton J.A., Eadon D.G. (1991). *Ultra-visible absorption spectra of the colloidal elements*, J. Chem. Soc. 87 Faraday Trans. (24, 3881–3891)

De Windt, W.; Aelterman, P.; Verstraete, W. (2005). *Bioreductive deposition of palladium (0) nanoparticles on Shewanella oneidensis with catalytic activity towards reductive dechlorination of polychlorinated biphenyls*. Environm. Microbiol., 7 (3), 314–325.

Egerton R.F. (2005). *Physical Principles of Electron Microscopy: An Introduction to TEM, SEM, and AEM*. Editor, Springer.

Fan F. R., Liu D. Y., Wu Y. F., Duan S., Xie Z. X., Jiang Z. Y., Tian Z. Q. (2008). *Epitaxial growth of heterogeneous metal nanocrystals: from gold nano-octahedra to palladium and silver nanocubes. J. Am. Chem. Soc.*, *130*, 6949–6951.

Ferrando R., Jellinek J., Johnston R.L. (2008). *Nanoalloys: from theory to applications of alloy clusters and nanoparticles*., Chem Rev., Mar;108(3):845-910

Ferrer D., Torres-Castro A., Gao X Sepulveda Guzman S., Ortiz Mendez U, Jose Yacaman M. (2007). *Three layer core-shell structure in bimetallic nanoparticles*. Nano letters 7, 1701. (ISSN: 1530-6984)

Frenkel A.I, Hills C. W., Nuzzo R.G. (2001). *View from the inside: Complexity of the atomic scale ordering in metal nanoparticles J. Phys. Chem. B*, *105*, 12689-12703.

Ghosh, S.K.; Kundu, S. & Pal, T. (2002). *Evolution, dissolution and reversible generation of gold and silver nanoclusters in micelle by UV-activation*. Bull. Mater. Sci. Vol.25, pp. 581-582

Hafner Bob, *Energy Dispersive Spectroscopy on the SEM: A Primer*, University of Minnesota, Twin Cities. Accessed January 2016. http://www.charfac.umn.edu/instruments/eds_on_sem_primer.pdf

Hayashi, H. & Hakuta, Y. (2010). *Hydrothermal Synthesis of Metal Oxide Nanoparticles in Supercritical Water. Materials*, Vol.3, pp. 3794-3817

Hosseinkhani B, Søbjerg LS, Rotaru AE, Emtiazi G, Skrydstrup T, Meyer RL. (2007). *Microbially supported synthesis of catalytically active bimetallic Pd-Au nanoparticles*. Biotechnol Bioeng;109(1):45-52

Husein, M.M. & Nassar, N.N. (2008). *Nanoparticle Preparation Using the Single Microemulsions Scheme. Current Nanoscience*, Vol.4, pp 370-380

Jellinek J. (2008). *Faraday Discuss*,. 138: p. 11.

Kharisov B., Kharissova O., Ortiz-Mendez U., (2012) Handbook of Less-Common Nanostructures, CRC Press.

Kim J.H., Chung H. W., Lee T.R. (2006). *Preparation and Characterization of Palladium Shells with Gold and Silica Cores*. *Chem. Mater*, 18(17): p. 4115.

Knecht M.R., Weir M.G., Frenkel A.I., Crooks R.M. (2008). *Structural Rearrangement of Bimetallic Alloy PdAu Nanoparticles within Dendrimer Templates to Yield Core/Shell Configurations*, *Chem. Mater.*, *20*, 1019-1028.

Kronberg B., Holmberg K. and Lindman B. (2014). *Surface Chemistry of Surfactants and Polymers*, First Edition, John Wiley & Sons

Larios E., Calderon L., Guerrero K., Pinedo E. Maldonado A., Tanori J. (2012). *Synthesis of core-shell (Pd-Au) bimetallic nanoparticles in microemulsions*. Journal of Dispersion Science and Technology, 33:9, 1360-1367.

LE-CSSS, Arizona State University, *High-Angle Annular Dark-Field (HAADF) Microscopy*. Accessed January 2016. (http://le-csss-dev.asu.edu/node/16).

Liu, H. B., Pal U., Medina, A., Maldonado C., Ascencio J.A. (2005). *Structural incoherency and structure reversal in bimetallic Au-Pd nanoclusters*, *Phys. Re*V*. B*, *71*, 075403.

Liu W., Qian T., Hiang H. (2014). *Fe nanoparticles: recent advances in synthesis and application in catalytic elimination of environmental pollutants*, Chemical Engineering Journal, 236, 448–463.

Lopez-Quintela, M.A. (2003). *Synthesis of nanomaterials in microemulsions: formation mechanism and growth control*. Curr. Opin. Coll. Int. Sci. Vol.8, pp. 137-144

Lopez-Sanchez, JA and Dimitratos, N and Miedziak, P and Ntainjua, E and Edwards, JK and Morgan, D and Carley, AF and Tiruvalam, R and Kiely, CJ and Hutchings, GJ (2008). *Au-Pd supported nanocrystals prepared by a sol immobilisation technique as catalysts for selective chemical synthesis*. Physical Chemistry Chemical Physics, 10 (14). pp. 1921-1930. ISSN 14639076 (ISSN)

Maclennan A, (2012). *Investigation of Au, Pd, and AuPd nanoparticle catalysts for alcohol oxidation reactions,* , University of Saskatchewan.

McNab W. W.; Ruiz R.; Reinhard M. (2000). *In-situ destruction of chlorinated hydrocarbons in groundwater using catalytic reductive dehalogenation in a reactive well: Testing and operational experiences*. Environ. Sci. Techno, 34 (1), 149–153.

Mohanty, U.S. (2011). *Electrodeposition: a versatile and inexpensive tool for the synthesis of nanoparticles, nanorods, nanowires, and nanoclusters of metals*, J. Appl. Electrochem., Vol. 41, pp. 257-270

Nanocomposites - Classification Types, Potential Applications, Interactions and Novel Nanocomposites (2007), AZoNano.

Nutt M. O., Hughes J. B., Wong M. S. (2005). *Designing Pd-on-Au bimetallic nanoparticle catalysts for trichloroethene hydrodechlorination*. Environ. Sci. Technol., 39 (5), 1346–1353.

Okamoto H., Massalski T. B. (1985). *Bull. Alloy Phase Diagrams.*

Pérez-Tijerina, E.; Gracia Pinilla, M.; Mejía-Rosales, S.; Ortiz-Méndez,U., Torres, A. & José-Yacamán, M. (2008). *Highly size-controlled synthesis of Au/Pdnanoparticles by inert-gas condensation*, Faraday Discuss., Vol.138, pp. 353-362

Prasad, P.N., Mark, J.E., Kandil, S.H., Kafafi, Z.H. (1998). *Science and Technology of Polymers and Advanced Materials: Emerging Technologies and Business Opportunities*, Springer US.

Sanchez-Dominguez, M.; Boutonnet, M. & Solans, C. (2009). *A novel approach to metal and metal oxide nanoparticle synthesis: the oil-in-water microemulsion reaction method*, J Nanopart Res, Vol.11, pp. 1823–1829

Schneider C.A., Rasband W.S., Eliceiri K.W. (2012). *NIH Image to ImageJ: 25 years of image analysis*. *Nat Meth*, *9*, 671-675.

Scott R. W. J., Wilson O. M., Oh S. K., Kenik E. A., & Crooks R. M. (2004). *Bimetallic palladium - Gold dendrimer-encapsulated catalysts*. Journal of the American Chemical Society, 126(47), 15583-15591

Shevchenko E.V., Bodnarchuk M.I., Kovalenko M.V., Talapin D.V., Smith R.K., Aloni S., Heiss W., Alivisatos A.P. (2008). *Gold/Iron Oxide Core/Hollow-Shell Nanoparticles*. Adv. Mater., 20, 4323-4329 .

Shi W., Casas J., Venkataramasubramani M. And Tang L. (2012). *Synthesis and Characterization of Gold Nanoparticles with Plasmon Absorbance Wavelength Tunable from Visible to Near Infrared Region*, Nanomaterials, Volume 2012.

Solanki, J.N. & Murthy, Z.V.P. (2010). *Highly monodisperse and sub-nano silver particles synthesis via microemulsion technique*, Colloids and Surfaces A: Physicochem. Eng. Aspects, Vol.359, pp. 31–38

Sonawane, R.,S. & Dongare, M.,K. (2006). *Sol–gel synthesis of Au/TiO_2 thin films for photocatalytic degradation of phenol in sunlight*, J. Mol. Cat. A,Vol.243, pp. 68–76

Song, K.C.; Lee; S.M., Park; T.S. & Lee, B.S. (2009). *Preparation of colloidal silver nanoparticles by chemical reduction method*. Korean J. Chem. Eng. Vol.26, pp. 153-155

Tamamushi, B. and Watanabe, N. (1980). *The formation of molecular aggregation structures in ternary system: Aerosol OT / water / iso-octane*, Colloid Polyme Sci., 258: 174–178.

Turkevich J, Stevenson P., Hiller J. (1951). Discuss. of the Faraday Soc., 11: p. 55.

Venezia A. M., Liotta L. F., Pantaleo G., La Parola V., Deganello G., Beck A., Koppany Z., Frey K., Horvath D., Guczi L. (2003). *Activity of SiO_2 supported gold-palladium catalysts in CO oxidation*. Appl. Catal., 251 (2), 359–368.

Wilson Adria R., Sun Keyi, Chi Miaofang, et al., (2013). *From core-shell to alloys: The preparation and characterization of solution-synthesized AuPd nanoparticle catalyst*, J. Phys. Chem. C, 117, 17557−17566.

Wu M. , Chen D. and Huang T. (2001). *Synthesis of Au/Pd Bimetallic Nanoparticles in Reverse Micelles*, *Langmuir*, 2001, *17* (13), pp 3877–3883

Yasar-Inceoglu O., Lopez T., Farshihagro E., and Mangolini L. (2012). *Silicon Nanocrystal Production through Non-thermal Plasma Synthesis: a Comparative Study Between Silicon Tetrachloride and Silane Precursors*, *Nanotechnology*, Vol. 23, No. 25, 255604.

Zhan G., Huang J., Du, M. et al., (2011). *Green synthesis of Au-Pd bimetallic nanoparticles: single-step bioreduction method with plant extract*, Materials Letters, 65, 2989–2991

Zhang, W.; Qiao, X.; Chen, J. & Wang, H. (2006). *Preparations of silver nanoparticles in water-in-oil AOT reverse micells*. J. Colloid Interf Sci, Vol.302, pp. 370-373

Zhang, W.; Qiao, X. & Chen, J. (2007). *Synthesis of silver nanoparticles—Effects of concerned parameters in water/oil microemulsion*. Mater. Sci. Eng. B, Vol.142, pp. 1–15

Zhao D., Xu B.Q. (2006). *Enhancement of Pt utilization in electrocatalysts by using gold nanoparticles*, Angew. Chem. Int. Ed 45, 4955.

Zielińska-Jurek, A., Reszczyńska J., Grabowska E. and Zaleska A. (2012). *Nanoparticles Preparation Using Microemulsion Systems, Microemulsions - An Introduction to Properties and Applications*, Dr. Reza Najjar (Ed.).

Appendix

ACADEMIC ACTIVITIES AS A RESULT OF THIS INVESTIGATION

1. PARTICIPATION IN THE “X COLOQUIO BIENAL EN CIENCIA DE MATERIALES” in Hermosillo, Sonora, Mexico, during March 8th, 2013. Presentation of poster entitled: “Synthesis of core-shell (Pd-Au) bimetallic nanoparticles in microemulsions”. Gálvez J., Larios E., Calderon L., Guerrero K., Pinedo E. Maldonado A., Tanori J.

2. PARTICIPATION IN THE NIM (Nanosystems Initiative Munich) SUMMER RESEARCH PROGRAM 2013 in Munich, Germany, at the Walter Schottky Institute of The Technical University of Munich, from July to August 2013, working in the Project: “Functionalization of diamond surfaces for protein-hybrid systems”. Project Supervisor: José Garrido, Research Mentor: Roberta Caterino.

3. PRESENTATION OF THE PROJECT: “Functionalization of diamond surfaces for protein-hybrid systems” at the Walter Schottky Institute of The Technical University of Munich on August 28th, 2013. Gálvez J., Garrido J., Caterino R.,

4. DELIVERING OF THE FINAL REPORT OF THE PROJECT: “Functionalization of diamond surfaces for protein-hybrid systems” in October, 2013, to Departamento de Polímeros y Materiales de la Universidad de Sonora. Gálvez J., Garrido J., Caterino R.,